CHAPTER 8

# *Detection and Measurement Techniques*

**Contents**


| | | | |
|---|---|---|---|
| 8.1. | Track measurements | | 193 |
| | 8.1.1. | Cloud and bubble chambers | 193 |
| | 8.1.2. | Solid state nuclear track detectors | 194 |
| 8.2. | General properties of detectors | | 198 |
| | 8.2.1. | Pulse generation | 199 |
| | 8.2.2. | Basic counting systems | 201 |
| | 8.2.3. | Pulse shape and dead time | 202 |
| 8.3. | Gas counters | | 204 |
| | 8.3.1. | Ion chambers | 206 |
| | 8.3.2. | Proportional counters | 208 |
| | 8.3.3. | Geiger-Müller counters | 210 |
| 8.4. | Semiconductor detectors | | 212 |
| | 8.4.1. | Surface barrier detectors | 214 |
| | 8.4.2. | Lithium-drifted detectors | 215 |
| | 8.4.3. | Intrinsic detectors | 217 |
| 8.5. | Scintillation detectors | | 218 |
| | 8.5.1. | Gas scintillator detectors | 220 |
| | 8.5.2. | Liquid scintillator detectors | 221 |
| | 8.5.3. | Solid scintillator detectors | 221 |
| 8.6. | Cerenkov detectors | | 222 |
| 8.7. | Electronics for pulse counting | | 223 |
| | 8.7.1. | Preamplifiers | 223 |
| | 8.7.2. | Amplifiers | 224 |
| | 8.7.3. | Single channel analyzers | 225 |
| | 8.7.4. | Counters and rate meters | 225 |
| | 8.7.5. | Multichannel analyzers | 226 |
| | 8.7.6. | γ-spectrometry | 226 |
| 8.8. | Special counting systems | | 229 |
| 8.9. | Absolute disintegration rates | | 231 |
| 8.10. | Sample preparation | | 233 |
| 8.11. | Statistics of counting and associated error | | 233 |
| 8.12. | Exercises | | 237 |
| 8.13. | Literature | | 237 |


Although animals have no known senses for detection of nuclear radiation, it has been found that sublethal but large radiation fields can affect animals in various ways such as disturbing the sleep of dogs or causing ants to follow a new pathway to avoid a hidden radiation source. Apollo astronauts observed scintillations in their eyes when their space

ship crossed very intense showers of high energy cosmic rays. People who have been involved in criticality accidents experiencing high intensities of n and γ have noted a fluorescence in their eyes and felt a heat shock in their body.

However, we are not physiologically aware of the normal radiation fields of our environment. In such low fields we must entirely rely on instruments.

The ionization and/or excitation of atoms and molecules when the energies of nuclear particles are absorbed in matter is the basis for the detection of individual particles. Macroscopic collective effects, such as chemical changes and heat evolution, can also be used. The most important of the latter have been described before because of their importance for dose measurements (e.g. the blackening of photographic films and other chemical reactions, excitation of crystals (thermoluminescence), and heat evolved in calorimeters; Ch. 7).

In this chapter we consider only the common techniques used for detection and quantitative measurement of *individual* nuclear particles. We also discuss the problem of proper preparation of the sample to be measured as well as consideration of the statistics of the counting of nuclear particles necessary to ensure proper *precision* (i.e. how well a value is determined) and *accuracy* (i.e. agreement between measured and true value).

## 8.1. Track measurements

The most striking evidence for the existence of atoms comes from the observation of tracks formed by nuclear particles in cloud chambers, in solids and in photographic emulsions. The tracks reveal individual nuclear reactions and radioactive decay processes. From a detailed study of such tracks, the mass, charge and energy of the particle can be determined.

The tracks formed can be directly observed by the naked eye in cloud and bubble chambers, but the tracks remain only for a short time before they fade. For a permanent record we must use photography. On the other hand, in solid state nuclear track detectors (SSNTD), of which the photographic emulsion is the most common variant, the tracks have a much longer lifetime during which they can be made permanent and visible by a suitable chemical treatment. Because of the much higher density of the absorber, the tracks are also much shorter and often therefore not visible for the naked eye. Thus the microscope is an essential tool for studying tracks in solids.

### 8.1.1. *Cloud and bubble chambers*

The principle of a *cloud chamber* is shown in Figure 8.1. A volume of saturated vapor contained in a vessel is made supersaturated through a sudden adiabatic expansion. When ionizing radiation passes through such a supersaturated vapor the ionization produced in the vapor serves as condensation nuclei. As a result small droplets of liquid can be observed along the path of the radiation. These condensation tracks have a lifetime of less than a second and can be photographed through the chamber window. The density of the condensation depends on the ionization power of the projectile as well as on the nature of the vapor, which is often an alcohol or water. Cloud chamber photographs are shown in

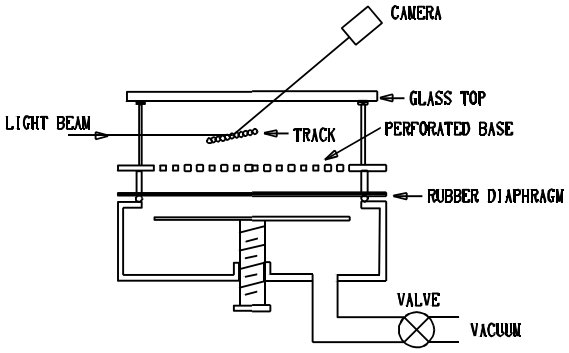


FIG. 8.1. Principle of a cloud chamber

Figure 6.5.

In a similar fashion *bubble chambers* operate with superheated liquids in which gas bubbles are produced upon the passage of ionizing radiation. The most commonly used liquid in bubble chambers is hydrogen, and, as a consequence, the chamber must be operated at low temperatures (23 K for $H_2$). Since the liquid medium in a bubble chamber is much denser than the vapor medium in a cloud chamber, the former are more suitable for studies of reactions of more energetic projectiles. The high energy p-p reaction shown in Figure 10.4 has been recorded in an 0.8 m diameter bubble chamber at Saclay, France; see also Figure 6.18.

### 8.1.2. *Solid state nuclear track detectors (SSNTD)*

The main types of SSNTD (or DTD, for dielectric track detector) are photographic emulsions, crystals, glasses, and plastics. Because the density of these materials is much higher than for the previous group (§8.1.1), nuclear particles can spend all their kinetic energy in these detectors, allowing identification of the particle. Since the SSNTD retains the particle path, they can be used to record reactions over a long time period. These advantages have made SSNTD especially valuable in the fields of cosmic ray physics, radiochemistry, and earth sciences.

*Nuclear emulsions* are similar to optical photographic emulsions. They contain AgBr crystals embedded in gelatin to which small amounts of sensitizing agents have been added. The AgBr content is as much as four times (i.e. 80% AgBr) greater than in optical film. Also the crystals are much smaller (developed grain 0.1 – 0.6 μm) and well separated. The emulsions come in thicknesses from a few μm up to 1 mm. Nuclear radiation passing through the emulsion causes ionization and excitation which activates the AgBr crystals, producing a latent image of the particle path. Upon development the activated crystals serve as centers for further reduction of silver, leading to visible grains. It is assumed that at least 3 silver atoms must be activated to produce a visible grain, while about 30 atoms are needed for normal blackening. Each activated grain seems to require about 2.5 eV to be absorbed on the average.

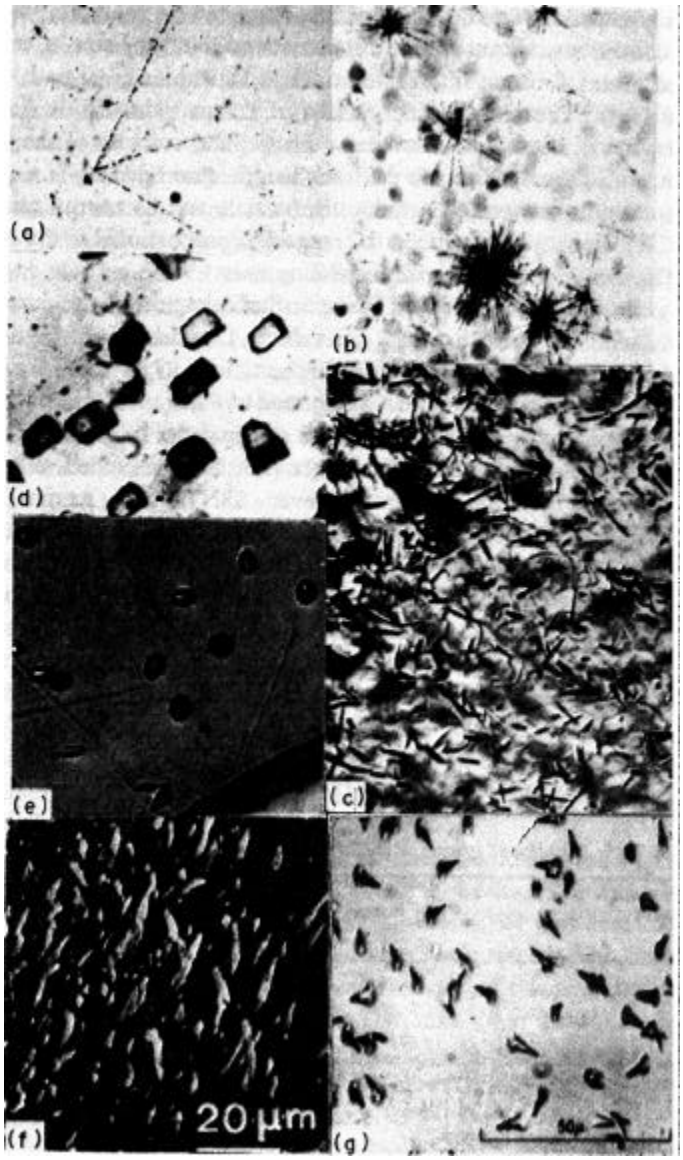


FIG. 8.2. Tracks of highly ionizing particles in solid absorbers. (a) Alpha-tracks originating in the same point in a nuclear emulsion. (Acc. to P. Cuer.) (b) Autoradiography of a lung showing deposits of inhaled plutonium. (Acc. to B. A. Muggenburg.) (c) Fission tracks in neutron irradiated apatite containing some evenly distributed uranium. (Acc. to E. I. Hamilton.) (d) Neutron-induced fission tracks in muscovite mineral. (Acc. to E. I. Hamilton.) (e) Neutron-induced fission tracks in volcanic glass recovered from deep sea sediments. (Acc. to J. D. Macdogall.) (f) Fission tracks in mineral from the Oklo mine. (Acc. to J. C. Dran *et.al.*) (g) Fission tracks from $^{252}Cf$ in Lexan polycarbonate. (From Fleischer, Price, and Walker.)

While the memory effect of the developed film is almost infinite, this is not the case for the latent image which slowly fades, depending on the number of originally activated silver atoms, the film type and external conditions like temperature, humidity, etc. When stored under ambient conditions, about 80% of the latent image disappears in half a year.

The developed grains form an interrupted track along the original path of the energetic particle (Fig. 8.2(a)). The specific energy loss of the particle, d$E$/d$x$ (i.e. the stopping power of the absorber), depends on the mass, charge, and velocity of the particle, and on the composition of the absorber. From the track length, grain density (i.e. grains per track length), and gap length between the grains, the particle and its energy can be determined (cf. §§6.3 and 7.1). For a given particle, the range $R$ is proportional to the energy as shown in Table 8.1. The range decreases with increasing mass of the particle and density of the absorber. The grain density depends on the specific ionization of the particle which does not vary linearly with the particle energy (or velocity), as seen from Figure 6.7; thus the grain density changes along the track.

Other solid material may be used as SSNTD instead of AgBr emulsions: *plastics* (cellulose nitrate and polycarbonate films), *glass*, *crystals*, etc. In order to make the tracks visible in the microscope the surface of the SSNTD must be polished and etched, usually with alkali.

Because of the natural radiation background, every SSNTD has a memory of past nuclear events, which must be erased as far as possible before a new exposure. In nuclear emulsions an α-radiation background of 20 – 60 tracks $cm^{-2}$ per day is normal. The technique of *background eradication* prior to exposure may consist of treating an emulsion with chromic acid, $H_2O_2$-vapor or heating (annealing) a glass plate. Because this technique more easily removes weak images, it may also be used after exposure, e.g. to remove fainter α-tracks from heavier fission tracks.

Let us consider some examples of uses of SSNTD. Tracks obtained under various conditions are shown in Figure 8.2.

Table 8.1. *Range of energetic high-ionizing particles in various solids*

| Particle | Energy (MeV) | Absorber (density) | Range (μm) |
|---|---|---|---|
| $^{1}H$ | 10 | Ilford C2 (3.8)[a] | 540 |
| $^{3}H$ | 10 | Ilford C2 (3.8)[a] | 230 |
| $^{4}He$ | 10 | Ilford C2 (3.8)[a] | 57 |
| $^{4}He$ ($^{214}Bi$) | 7.7 | Eastman NTA (3.6) | 38 |
| | | Mica (3.1) | 36 |
| | | Glass (2.5) | 41 |
| | | Water (1.0) | 60 |
| $^{4}He$ ($^{238}U$) | 4.2 | Mica (3.1) | 13 |
| $^{4}He$ (U-series) | | Pitchblende (7.0) | 23[b] |
| | | Carnotite (4.1) | 32[b] |
| $^{235}U$ Light fiss. fragm. | ~150 | Eastman NTC (~3.4) | 14 ~25 |
| $^{235}U$ Heavy fiss. fragm. | | Eastman NTC (~3.4) | 10.5 |
| $^{238}U$. Both fiss. fragm. | ~160 | Leopoldite (~4) | ~20 |

[a] Density of AgBr 6.47; of gelatin 1.31.
[b] Range of the predominating α-particles.

(i) As mentioned SSNTD has been used in cosmic ray experiments at high altitudes and in space journeys where memory effect and simple construction make them especially suitable. Many elementary particles have been discovered by this technique, notably the π- and μ-mesons. Figure 10.2 shows tracks of high energy cosmic ray particles, probably iron atoms, which have been stopped in Apollo astronaut helmets.

(ii) Nuclear reactions can be studied by SSNTD. The target material may either be regular atoms of the detector (H, O, Ag, Si, etc.) or material introduced into the matrix, e.g. thin threads of target metals or uranium atoms. The former have been used in high energy physics for hadron-induced reactions, and the latter for studying fission processes. From experiments with uranium the frequency of spontaneous fission of $^{238}U$ has been determined, and also the rate of ternary fission and emission of long range α's.

(iii) When emulsions are dipped into solution, some of the dissolved material is soaked up or absorbed in the emulsion. For example, if the solution contained samarium, some α-tracks of its spontaneous decay (decay rate 127 Bq $g^{-1}$) appear in the emulsion (cf. Fig. 8.2(a)). Since $^{147}Sm$ has an isotopic abundance of 15%, its half-life is calculated to be $1.1 \times 10^{11}$ y. The lower limit of detection is about 500 tracks $cm^2\ d^{-1}$, so quite low decay rates can be accurately measured, making this a valuable technique for determination of long half-lives.

(iv) $^{222}Rn$ is released through the earth's surface from uranium minerals. The amount released varies not only with the uranium content and mineral type, but also with the time of the day; variation from 1 – 75 Bq $l^{-1}$ has been registered during a 24 h period. To avoid this variation, cups containing a piece of plastic TD are placed upside down in shallow (0.5 – 1.0 m) holes for about 3 weeks, after which the SSNTD are etched and α-tracks from radon counted. Mineral bodies hundreds of meters underground can be mapped with this technique in great detail in a reasonably short time. The US Geological Survey uses the same technique to predict earthquakes; it has been observed that just before earthquakes the radon concentration first increases, then suddenly decreases, the minimum being observed about one week before the earthquake appears.

(v) The average radon concentration in houses can be measured by hanging a plastic film inside the house over a time period of some weeks. The film is returned to a laboratory where it is etched and the number of α-tracks per unit area counted.

(vi) Fission fragments make dense tracks in all solid material. The tracks are short and thick: in a crystal material like zircon (a common mineral of composition $ZrSiO_4$) they may not be more than $10^{-2}$ μm (10 nm) in diameter, and 10 – 20 μm in length. They are therefore not visible even in the best optical microscopes. Using scanning electron microscopy, it has been found that the hole formed retains the crystal structure or regains it (Fig. 8.2(d)). On the other hand, if the track is formed in glass, a gas bubble appears instead of a track (Fig. 8.2(e)); these slightly elongated bubbles can be distinguished from other completely spherical bubbles formed by other processes. To make the tracks visible, the specimen is embedded in a resin, then one surface is ground and carefully polished after which it is dipped in an acid, e.g. HF. Because of defects in the crystal structure along the fission track, the track and its close surroundings are attacked by the acid, and the diameter of the track increases a hundredfold to a micron or so. The tracks are then visible under a microscope with a magnification of 500 – 1000 ×.

This procedure has been used as an analytical tool for determination of uranium and plutonium in geological and environmental samples. In this technique, the sample (either

a ground and polished surface of a mineral, or a dust sample on tape) is firmly pressed against a photographic film, and the package is irradiated by slow neutrons. From the fission track count of the developed film the uranium or plutonium content can be calculated. Thus a Swedish shale was found to contain 4 ± 1 ppm U, and a bottom sediment in a Nagasaki water reservoir 0.44 ± 0.04 Bq $^{239}$Pu per kg sediment. In the latter case, the ratio between the number of fission tracks $N_{ft}$ and α-tracks $N_{\alpha t}$ from $^{239}$Pu is

$$N_{ft}/N_{\alpha t} = \sigma_f \phi/\lambda_\alpha \tag{8.1}$$

This technique is very useful for routine measurements of fissionable material in very low concentrations. Figure 8.2(c) shows fission tracks in uranium-containing mineral which has been exposed to neutrons.

Fission track counting is also important for dating of geological samples (Ch. 5) and for estimation of the maximum temperature experienced by sedimentary rocks. The latter is important in oil prospecting operations as the maximum temperature seems to be a useful indicator on whether to expect oil, natural gas or nothing. For too low temperatures neither oil nor gas is expected, for intermediate temperatures oil may be present and for high temperatures only natural gas. Temperature history information can obtained from a combination of age (estimated by other radioactive methods, cf. Ch. 5), uranium content of crystals of several minerals in the rock, their fission track count and track-length distribution caused by thermal annealing. Zircon, titanite and apatite are examples of three such minerals in order of increasing annealing temperature.

## 8.2. General properties of detectors

A nuclear particle entering a detector produces excitation and ionization, both of which can be used for detection. When the excitation is followed by fluorescent de-excitation (§§7.4 and 7.5.3) the light emitted can be registered by light-sensitive devices, e.g. the photomultiplier tube (PMT) which transforms the light into an electric current. Scintillation and Cerenkov detectors are based on light emission. A similar current is generated when production of *charge carriers* (i.e. ions, electrons and holes) takes place between the charged electrodes of a detector. Detectors based on the production of charge carriers are either gas-filled (ion chambers, proportional and Geiger-Müller tubes in which charge carriers are produced by ionization of a gas) or solid, usually semiconductor crystals. In the latter case electrons and holes are produced in pairs (§8.4).

An ionizing particle or photon will produce a collectable charge $\Delta Q$ in the detector

$$\Delta Q = 1.60 \times 10^{-19} E_{loss}\, \eta\, w^{-1} \tag{8.2}$$

where $E_{loss}$ is the total energy lost by the particle to the detector, $\eta$ is the collection efficiency, $w$ is the energy required for the formation of a pair of charge carriers in the detector medium, while the constant is the charge (Coulomb) of a single charge carrier (the pairs must be regarded as singles because they move in opposite direction in the electric field due to their opposite charges).

Because of the short duration of the absorption process for a single particle ($10^{-4}$ – $10^{-9}$ s) the short current, $i$, is referred to as a *pulse* of charge $\Delta Q$

$$i = \Delta Q/\Delta t \tag{8.3}$$

If this current passes through a resistor $R$ it will produce a voltage pulse (cf. (8.2))

$$\Delta V = R\,\Delta Q/\Delta t \tag{8.4}$$

The pulse is usually referred to as the *signal* (for the preamplifier). While the signal from semiconductor detectors is used as a charge pulse, most other detectors immediately convert the current to a voltage drop over a resistor. In either case, the output from the preamplifier is usually a voltage pulse. Preamplifiers are often integrated with the detector.

Pulse counting *per se* does not distinguish between different nuclear particles (α, β, γ, etc.) or between particles of different energy. Such distinction is obtained by choosing detectors of unique (or exceptionally high) sensitivity to the particles of interest. Energy analysis, if desired, is achieved by the accompanying electronic circuitry because the pulse charge or voltage ($\Delta Q$ or $\Delta V$) is proportional to the energy of the absorbed particle.

### 8.2.1. *Pulse generation*

We shall use Figure 8.3 to describe the formation of a voltage pulse. A detector is connected between points A and B. The detector has an *internal* resistance (because of the limited charge carrier mobility in the detector) and capacitance (because of mechanical construction), indicated by $R_i$ and $C_i$. Figure 8.3(a) does *not* show the physical design of the detector, but only its electrical equivalents; this will make it easier to understand its function. When a particle enters the detector it produces charge carriers (this is symbolized by the closing of switch S), and the collection of these at the electrodes gives a current which, together with a small current from the bias supply through $R_e$, flows through $R_i$ to ground. $R_e$ is the resistance between the detector anode and the positive terminal of the bias voltage supply (voltage $+ V_0$); the other terminal is grounded. We shall concentrate our interest on the potential $V_p$ at point P which is connected via the comparatively large capacitance $C_e$ to the output. In general $R_e > R_i$ (under conducting conditions), and $C_e \gg C_i$; for illustrative purposes we will assume $R_e = 50$ kΩ, $R_i = 10$ kΩ and $C_e + C_i = 100$ pF.

When S is open (no ionization in the detector), the potential at point P must be $V_p = V_0$, i.e. the potential of the bias voltage. At time $t = 0$, S is closed (production of charge carriers has occurred in the detector because of a nuclear particle), and the charge of $C_i + C_e$ flows through $R_i$ together with a small current from the bias supply through $R_e$. The potential in P decreases according to

$$V_p/V_0 = a\,(1 - e^{-bt}) + e^{-bt} \tag{8.5a}$$

where $a = R_i/(R_i + R_e)$, $b = (a\,R_e\,C)^{-1}$, and $C = C_i + C_e \approx C_e$. For $R_e = 50$ kΩ, $R_i = 10$ kΩ and $C = 100$ pF, $a = 1/6$ and $b = 12\,000$ s$^{-1}$. $1/b$ is referred to as the *time constant*

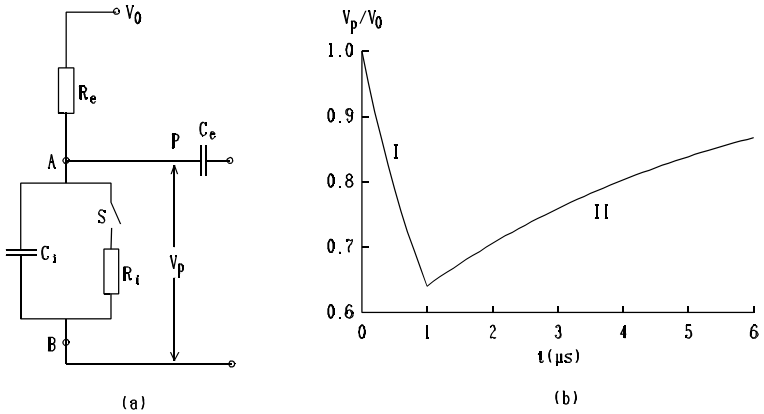


FIG. 8.3. (a) Equivalent circuit (b) pulse shape in point P.

of the system (the decay time of the charge of the system); in the time $1/b$ the voltage has dropped to $V_0/\mathbf{e}$. Assuming the charge collection ends after 1 μs this is equivalent to opening switch S at that time. The voltage in P has now fallen to its minimum value as indicated in Figure 8.3(b).

When S is opened charge starts building up on the capacitors by current flowing from the bias voltage through resistor $R_e$. The voltage in P begins to increase again according to

$$V_p / V_0 = 1 - (1 - V_m / V_0)\, e^{-t/(R_e C)} \tag{8.5b}$$

where $V_m$ is the voltage in P when the switch is opened again, $t$ is now the time after opening of S and $C = C_e + C_i$. If we assume $R_e = 50$ kΩ the voltage build-up will follow the climbing curve to the right of 1 μs in Figure 8.3(b). In practice, the current flow stops more gradually and the potential in P follows a smoother curve.

The voltage drop at P results in a negative voltage pulse after the capacitor $C_e$. In Figure 8.3(b) the voltage change at point P is more than 40% of the bias voltage; this is highly exaggerated, since the change is normally a very small fraction of the bias voltage. This is due to the fact that the current is carried only by the charge carriers formed in the detector. If the number of primary charge carriers formed is $n_i$, the charge transport $\Delta Q$ is

$$\Delta Q = -1.60 \times 10^{-19}\, n_i\, a \text{ (Coulomb)} \tag{8.6}$$

where $a$ is the multiplication factor (1 in solid state detectors, $\gg 1$ in gas-filled detectors). When $a < 1$ it has the same meaning as the collection efficiency η in (8.3). The maximum voltage drop is then

$$\Delta V \approx \Delta Q / C \tag{8.7}$$

If $10^5$ charge carrier pairs have formed in the detector and $C = 100$ pF, then $\Delta V = 0.16$ mV. In practice the effective voltage drop $\Delta V_{\text{eff}}$ is somewhat less than the calculated $\Delta V$.

### 8.2.2. *Basic counting systems*

The block diagram of Figure 8.4 indicates the most common components in a measuring circuit. The detector (in its shield A) is connected to a stabilized bias voltage power supply B which furnishes the potential difference necessary for the detector to operate. The magnitude and type of the signal from the detector varies, depending on the type of detector, for the type of circuit illustrated in Figure 8.3 from a few hundred microvolts to several volts. In most cases it is necessary or preferable to have a *preamplifier* connected directly to the detector, cf. §8.7.1. The preamplifier often increases the pulse size to the 0.1 – 10 V preferred for the auxiliary system. This initial amplifier also supplies the power needed to drive the load presented by the connecting cable and input impedance of the *main amplifier* C. The total gain in the system may vary from 10 for a Geiger–Müller counter to $10^4$ for some solid state detectors.

A limit is set on the voltage gain of an amplifier by the presence of electronic noise at the amplifier input due to thermal noise in the detector and preamplifier input stage, microphonics, and components which cause small, random voltage changes. This noise is amplified with the signal and can mask small pulses from the detector. Some of the noise may be eliminated by proper design and operation of the electronic circuitry, but a small inherent noise is always present (Fig. 8.5(a) and §8.7.1). The *signal to noise ratio* is a ratio of output pulse (for a given input signal) to the noise level at the output. Noise pulses can be rejected by a *discriminator* D which serves as a filter to allow only pulses of a certain minimum size to be passed on to the rest of the system; in Figure 8.5(a) the discriminator rejects all pulses below the dashed line. The signal pulse, after amplification, is sufficiently large to operate the electronic *counter* H in Figure 8.4 causing registration of the pulses.

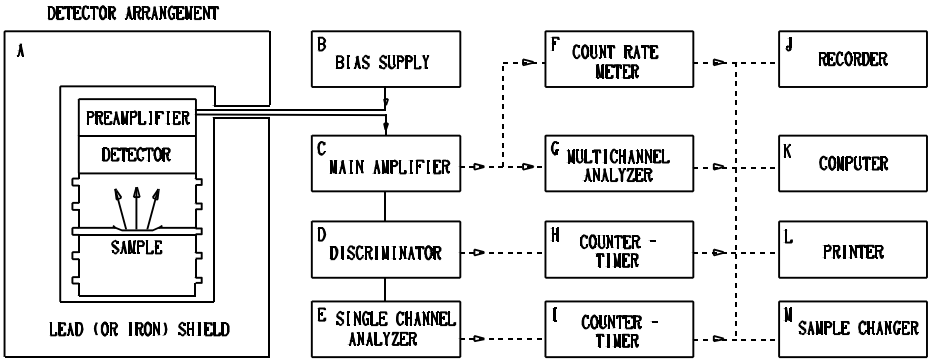


FIG. 8.4. The most common pulse-type measuring units and combinations.

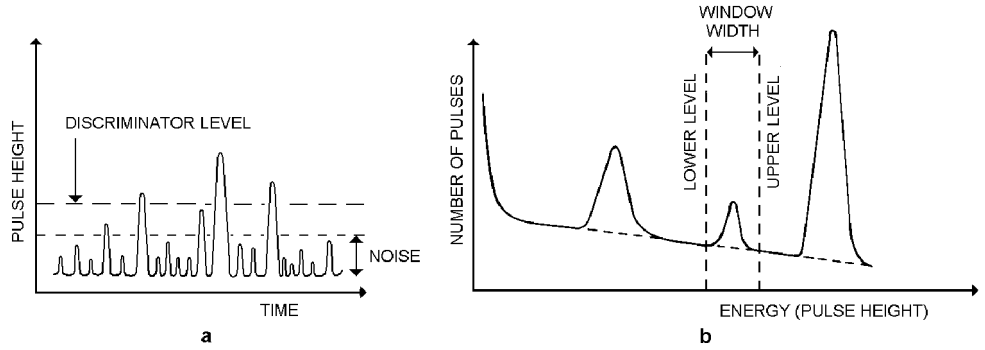


FIG. 8.5. Idealized pulse spectrum obtained (a) from a shaping amplifier, and (b) from a multichannel analyzer using a solid state detector. The figure shows the effect of different discriminator settings.

In modern counters the number of pulses counted are often shown on light-emitting diode (LED), gas-plasma, or liquid crystal displays.

### 8.2.3. *Pulse shape and dead time*

From Figure 8.3(b) it is obvious that it takes some time to restore proper measuring conditions. Such conditions may be assumed to have occurred when the potential $V_p$ has returned above a certain level. During the first part of this time the detector is unable to collect a new charge because working conditions have not been sufficiently restored. This

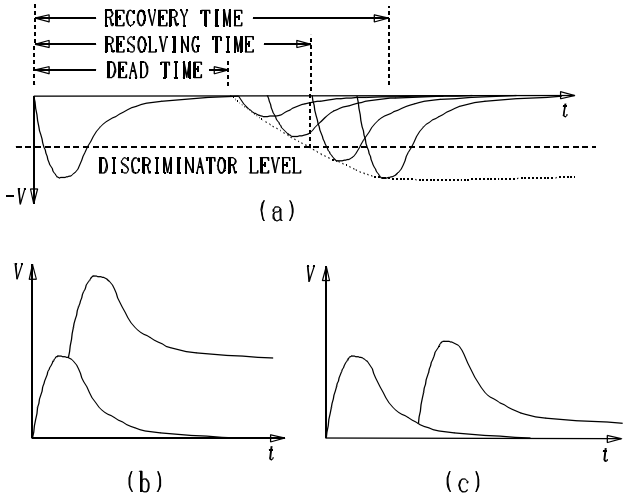


FIG. 8.6. Effects of short interval between events registered in detectors. (a) G.M. tube, (b) peak pile-up and (c) tail pile-up for fast detectors.

time, which in the figure is something like 10 μs, any new events would not produce a pulse crossing the discriminator level. This interval is properly called *dead time*, see Figure 8.6. Somewhat later the initial operating conditions are still not fully restored but the detector is now able to produce a pulse of larger magnitude which triggers the discriminator. Still later, after the *recovery time*, the initial conditions are restored. If the second event occur within a short time, *peak pile-up* will occur. At a somewhat later time the new pulse overlaps with the tail of the pulse from the previous event causing so called *tail pile-up*. Pulse pile-up may make two or more closely spaced events look like a single more energetic event, Figure 8.6. The time needed to separate two events is referred to as *resolving time* (for simplicity dead time and resolving time will be used as synonyms in this text). Thus the detector and measuring circuit needs a certain time to register each individual event separately with correct magnitude. In many cases the measuring circuitry is much faster than the detector and the dead time is a function of the detector only. Since radioactive decay is a statistical random process and not one evenly spaced in time, see §8.11, even for relatively low count rates a certain percentage of events will occur within the resolving time of the system. In order to obtain the true count rate it is necessary to know the correction that must be made for this *random coincidence loss*. In systems using a MCA for pulse height analysis, the MCAs pulse conversion time is usually determining the system dead time and not the detector.

Two different models exist for the dead time of counting systems depending on system behavior after a pulse. In a *nonparalyzable* system the pulses following the first within the dead time are lost, but the system is ready to accept another event immediately after the dead time has expired. The fraction of all real time during which the system is dead is then given by the product between the registered count, $R_{obs}$, and the dead time, $t_r$. The true number of events, $R_{corr}$, is then given by

$$R_{corr} = R_{obs}/(1 - R_{obs}\, t_r) \tag{8.8a}$$

In a *paralyzable* system each event starts a new dead time period whether or not it generates an output signal. This, in combination with the time distribution of radioactive decays (8.21), yields the following implicit expression for the true number of counts

$$R_{obs} = R_{corr}\, e^{-R_{corr}\, t_r} \tag{8.8b}$$

At very low count rates it can be shown the result is independent of the type of system, i.e. $R_{obs} \approx R_{corr}\,(1 - R_{corr}\, t_r)$. However, the behavior of these two system types at high count rates are different. A nonparalyzable system shows an asymptotic approach to a maximum count rate with increasing source strength whereas the count rate on a paralyzable system passes through a maximum and then decreases again. Hence each reading on a paralyzable system corresponds to one of two values, one low and one high. Dangerous mistakes can occur by misinterpreting the reading from a paralyzable dose rate meter.

The simplest technique for measuring the resolving time $t_r$ of a nonparalyzable counting system uses a method of matched samples. Two samples of similar counting rates are counted separately and then together. The combined sources should give about 20% fractional dead time, $R_{obs}\, t_r$. From the difference between the measured count rate of the

pair together and the sum of their individual rates, the resolving time is calculated using the equations:

$$x = R_a R_b - R_{ab} R_0$$

$$y = R_a R_b (R_{ab} + R_0) - R_{ab} R_0 (R_a + R_b)$$

$$z = y(R_a + R_b - R_{ab} - R_0)/x^2$$

$$t_r = x[1 - (1 - z)^{1/2}]/y \qquad (8.9)$$

where $R_a$, $R_b$, and $R_{ab}$, are the measured count rate of samples a and b separately, a and b together, respectively. $R_0$ is the background count rate for the system. The correction for the resolving time can then be made according to (8.8a).

A more accurate technique is based on the use of a short-lived radionuclide, e.g. $^{99m}$Tc or $^{116m}$In. The count rate is then measured a number of times during at least one half-life with the source left untouched in position all the time. When the background count rate can be neglected (which is usually the case) combining (8.8a) with the equation for radioactive decay gives after some algebra

$$R_{obs}\, e^{\lambda t} = R_0 - R_0\, t_r\, R_{obs} \qquad (8.10)$$

where $t$ is the time of measurement, $\lambda$ the decay constant and $R_0$ the initial count rate. A plot of $R_{obs}\, e^{\lambda t}$ as function of $R_{obs}$ should yield a straight line with slope $-R_0\, t_r$ and intercept $R_0$ on the vertical axis. The dead time is then obtained as the absolute value of slope divided by intercept. If the plotted data deviates strongly from a straight line it indicates that the system investigated is paralyzable.

## 8.3. Gas counters

All gas-filled counters are in principle ion chambers (with the exception of the less common gas scintillation counters). The ionization produced in an ion chamber by a single nuclear particle produces too low a charge pulse to be easily detectable except for α- particles. However, an ion chamber can be designed so that the number of ion pairs formed in each event is multiplied greatly.

Consider an ion chamber with a hollow cylindrical cathode and a thin central wire as an anode (Fig. 8.8(a) shows an old type GM-tube). The ion pairs formed in the gas by the passage of the ionizing radiation are separated from each other by their attraction to the electrodes. The small, very mobile electrons are rapidly collected on the anode, which is maintained at a high positive potential above ground, ≥ 1000 V. Most of the voltage pulse which appears on the anode arises by induction by the positive ions as they move away from the immediate region of the anode. This step is responsible for the rise time of the pulse, curve I in Figure 8.3(b). The potential decrease is only momentary as the anode is rapidly recharged by the power supply. The time necessary to restore the original potential

is a function of the decrease in electric field near the anode due to the build-up of a layer of slow-moving positive ions, and of the time constant circuitry (curve II in Fig. 8.3(b)).

The electric field strength at a distance $x$ from the anode is proportional to $1/x$. If the applied voltage of a cylindrical chamber of 1 cm radius is 1000 V, the potential in the immediate vicinity of a center wire of 0.0025 cm diameter is approximately $7 \times 10^4$ V cm$^{-1}$. As the primary electrons reach the vicinity of this high field and increase their kinetic energy, they cause secondary ionization which increases the pulse detected at the wire anode. The collected charge is given by (8.2), where $a$, *the gas multiplication factor*, is $\gg 1$.

This gas multiplication factor varies with the applied voltage as illustrated in Figure 8.7. In region II of the curve a flat plateau over a relatively wide voltage range is observed. Prior to the attainment of the threshold voltage for the plateau, the ions would not have sufficient *drift velocity* to prevent elimination of some ion pairs by recombination. Throughout the plateau range the drift velocity is sufficient to make recombination negligible and since secondary ionization is not present, $a = 1$. Ionization chambers operate in this voltage region. In region III the electrons from the primary ion pairs receive sufficient acceleration to produce additional ionization and the process of gas multiplication ($a > 1$) increases the number of collected charges. This is the region of *proportional counter operation* as the pulses are proportional in size to the energy deposited in the detector by the passage of the initial radiation. Region IV is the one used for *Geiger-Müller counter* (or GM counter) operation. In this region the gas multiplication is very high ($\geq$

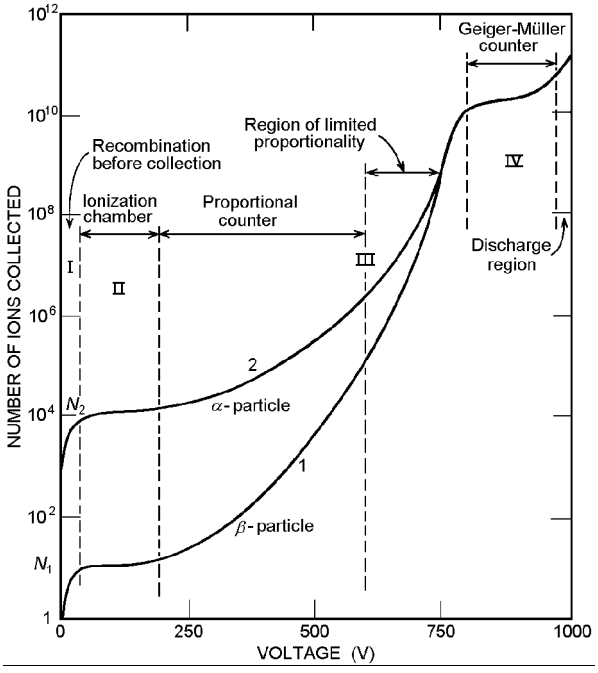


FIG. 8.7. Number of ion pairs formed in a gas-filled ionization chamber with a thin wire anode as function of anode voltage. (Acc. to C. G. Montgomery and D. D. Montgomery.)

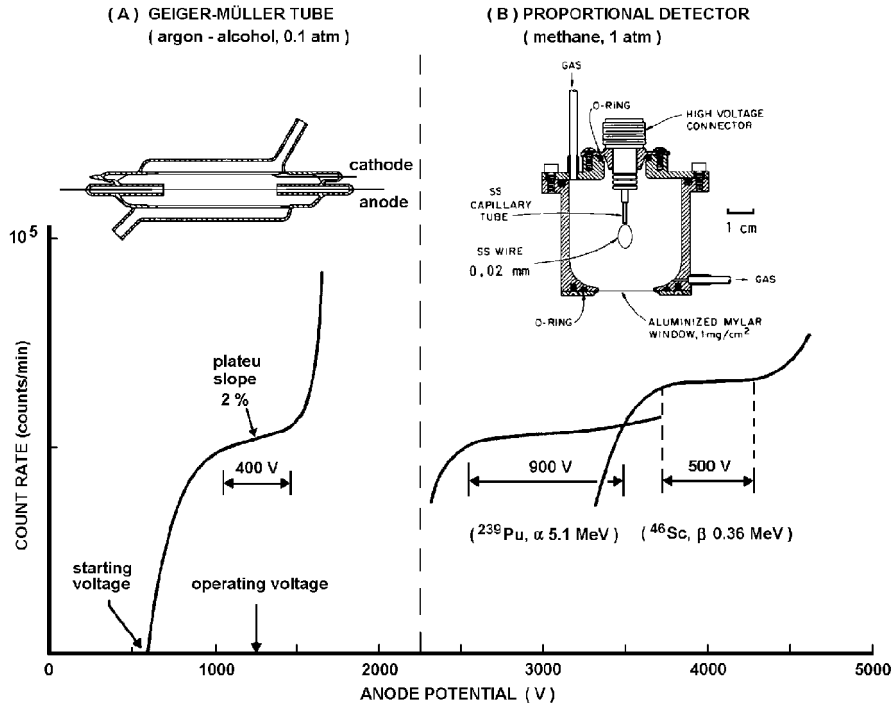


FIG. 8.8. Characteristics for GM and proportional counter tubes. The GM tube (a) is designed for flowing liquids. The proportional tube (b) uses a flowing counting gas.

$10^6$) and the pulse size is completely independent of the initial ionization. Beyond region IV continuous discharge in the detector occurs.

### 8.3.1. *Ion chambers*

The ion chamber is a gas-filled space between two electrodes. In Figure 8.9(a) the electrodes are two parallel plates, but another common geometrical arrangement uses the cathode as a hollow cylinder and the anode as a thin wire in its center, e.g. the GM tube in Figure 8.8(a). In other chambers the chamber walls serve as the cathode with a thin wire loop as anode as illustrated in Figure 8.8(b). The chamber may be designed for recording radiation reaching it from the outside, or it may be used for measuring radioactive samples placed within it. Some chambers have additional electrodes, usually a thin central grid to improve measuring conditions. The anode is kept at a positive potential 100-1000 V above the cathode.

Ions and electrons formed in the gas by nuclear radiation move towards the electrodes where they are discharged. If the gas is pure argon, only $Ar^+$ and $e^-$ are formed. The electrons move rapidly towards the anode, and then through the electrical circuitry, as

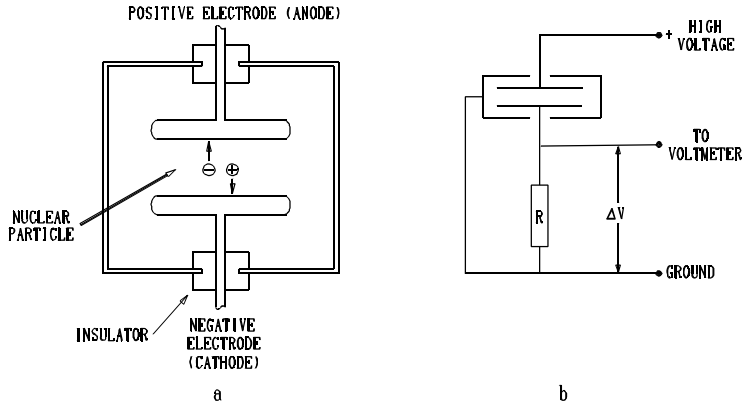


FIG. 8.9. (a) A parallel plate ionization chamber and (b) its measuring circuitry.

shown in Figure 8.9(b), over the resistor $R$ towards the cathode where they neutralize the argon ions: $Ar^+ + e^- \rightarrow Ar$. The gas is therefore not used up. The current $i$ through the chamber and through the resistor $R$ causes a voltage drop $V$,

$$V = R\,i \tag{8.11}$$

which can be continuously recorded by a sensitive voltmeter. If the current or voltage drop, $\Delta V$, is measured as a function of the voltage $V$ applied over the electrodes, it is found that the current (or $\Delta V$) increases with $V$ up to a saturation value. The reason for this is that at low voltages some of the positive ions formed initially by the radiation recombine with the electrons, reducing the collected charge. With higher voltages the cations and electrons separate more rapidly with less recombination, and at saturation value essentially no recombination occurs. The ionization chamber will always be operated at saturation voltage.

Suppose a 100 kBq $\alpha$-sample is placed within an argon-filled chamber of sufficient size that all the 5 MeV $\alpha$'s emitted are stopped in the gas volume. The saturation ion current will be found to be:

$$i = 1.60 \times 10^{-19} A E_{\text{loss}} \eta \psi_{\text{geom}} w^{-1} \tag{8.12}$$

where $A$ is the radioactivity of the sample in Bq, $E_{\text{loss}}$ is the total energy lost per particle ($5 \times 10^6$ eV) to the detector, $\eta$ is the collection efficiency, $\psi_{\text{geom}}$ is the geometric efficiency (for a thin solid sample we shall assume it to be half of a full sphere, i.e. 0.50), $w$ is the energy required for the formation of an ion pair in the gas (for argon 26 eV), while the constant is the charge (Coulomb) of a single ion (the ion pairs must be regarded as single charges): thus $i = 1.54 \times 10^{-9}$ A. With a resistor of $10^9\ \Omega$, the voltage drop $\Delta V$ is 1.5 V.

Two types of ion chamber are common: (i) Simple, portable, rugged instruments with resistors $\leq 10^{13}\ \Omega$. With these, radiation intensities of $\geq 10^3\ \beta\ s^{-1}$ and of $\geq 10^5\ \gamma\ s^{-1}$ can be measured. They are usually calibrated in dose rate (e.g. Gy $h^{-1}$) and used for radiation protection measurements under field conditions (*dose rate meters*). (ii) Advanced, very

sensitive instruments, with very high resistors (~ $10^{15}$ Ω) or special circuitry as in the vibrating reed electrometer. The chamber must always be designed with extreme care to avoid leaking currents from the anode over the chamber casing to the cathode. One way to minimize this is to ground the casing, as shown in Figure 8.9(b). In the best of these instruments, currents as low as $10^{-18}$ A can be measured, corresponding to less than 1 α $h^{-1}$, 10 β $min^{-1}$, or 10 γ $s^{-1}$. These instruments are best suited for measurement of radioactive gases, like tritium or radon in nature.

The *beta-current neutron detector* is a solid state ion chamber which is used in nuclear reactor technology. It consists of an emitter in which a nuclear reaction occurs, leading to the emission of primary $\beta^-$ particles (e.g. through the reaction ( $^{103}Rh(n,\gamma)^{104}Rh(\beta^-, 4.2\ s)\ ^{104}Pd$) or secondary electrons (e.g. through absorption of the prompt γ's emitted in the neutron capture). These electrons represent a current and are collected by a collector. The radioactive decay type detectors have a response time depending on the product half-life, which the capture-γ detectors lack. These detectors have a limited lifetime; for the $^{59}Co(n,\gamma)^{60}Co$ it amounts to 0.1% per month at $10^{13}$ n $cm^{-2}s^{-1}$. The lifetime depends on the $\sigma_{n\gamma}$ value (37 b for $^{59}Co$, 146 b for $^{103}Rh$).

### 8.3.2. *Proportional counters*

Values of *a* of $10^3$ – $10^5$ are commonly achieved in proportional counter operation. If $a = 10^3$, essentially all the gas multiplication occurs within 10 mean free path lengths from the wire for the electron in the gas ($2^{10} = 1024$). At 1 atm the mean free path length is approximately $10^{-6}$ m, which means that the gas multiplication occurs within 0.01 mm of the wire.

The gas multiplication factor varies with the applied voltage but for a given voltage *a* is constant so the detector pulse output is directly proportional to the primary ionization. As a result it is possible to use a proportional counter to distinguish between α- and β-particles and between identical particles of different energies inasmuch as different amounts of primary ionization are produced in these cases.

The output pulse in proportional counter operation is not dependent on the collection of the positive ions by the cathode. Consequently the rate of detection depends on the time necessary for the primary electrons to drift into the region of high field strength near the anode wire. As a result, proportional counters have a much shorter resolving time than ion chambers which depend on the slow-moving positive ions. In fact the detector tube in a proportional counter can amplify a new pulse before the positive ion cloud of the previous pulse has moved very far if the new ionization occurs at a different location on the center wire. Time intervals necessary to enable the counter to measure two distinct pulses can be as low as 0.2 – 0.5 μs. Frequently the associated measuring equipment is a greater determinant of the resolving time than the detector itself. If, however, a proportional counter is being used for the measurement of particle energies, any residual positive ion cloud must have time to drift an appreciable distance before a new pulse is generated. In this case the resolving time is closer to 100 μs.

Counting gases consists usually of one of the noble gases mixed with a small amount of polyatomic gas. The latter makes the gas multiplication factor less dependent on applied voltage, and increases the speed of electron collection. Typical counting gas mixtures are

90% Ar + 10% $CH_4$ ("P-gas") and 96% He + 4% i-$C_4H_{10}$ ("Q-gas"). Many other pure gases or combinations are possible, but molecules which readily attach electrons must be avoided. Figure 8.8(b) shows a proportional counter tube using pure $CH_4$ and the tube characteristics (i.e. count rate versus voltage) for $^{239}$Pu α-particles and for $^{46}$Sc β-particles entering through the thin aluminized mylar window.

The gas mixture and electrodes may be separated by a thin window from the radioactive sample, or the counter may be operated windowless. For windowless operation, after insertion of the sample the chamber must be flushed with gas to eliminate all the oxygen and water vapor as these molecules absorb electrons readily to form negative ions and, by so doing reduce the pulse size. For α- and β-particles whose ranges do not exceed the dimensions of the chamber, windowless counters are often referred to as $2\pi$ counters since a solid angle of $2\pi$ is subtended above the sample. In these cases, with proper care, the measured count rate is very close to 50% of the true disintegration rate. Such windowless proportional counters are very useful for measuring low energy radiation such as the β- emissions of $^{14}$C and $^{3}$H, and for absolute counting. Figure 8.10 shows a $4\pi$ proportional counter in which the sample is inserted in the middle between the two half-domes (cathodes).

Proportional counters can be used also for *neutron detection* by using a gas containing nuclei that capture neutrons and in the nuclear reaction produce charged particles, e.g. $^{10}$B or $^{3}$He. In $BF_3$-counter the gas is $BF_3$, usually enriched in $^{10}$B. With neutrons the reaction

$$^{10}\mathrm{B} + \mathrm{n} \rightarrow {}^{7}\mathrm{Li} + {}^{4}\mathrm{He} \qquad (Q = 2.78\ \mathrm{MeV})$$

occurs (cf. Ch. 14). The ionization of the two products produces a heavy pulse, which is easy to discriminate against an intense γ-background. Some properties of a $BF_3$ neutron detector are given in Table 8.2. From Figure 14.4 it is clear that the $BF_3$ counter has a higher efficiency for thermal than for fast neutrons.

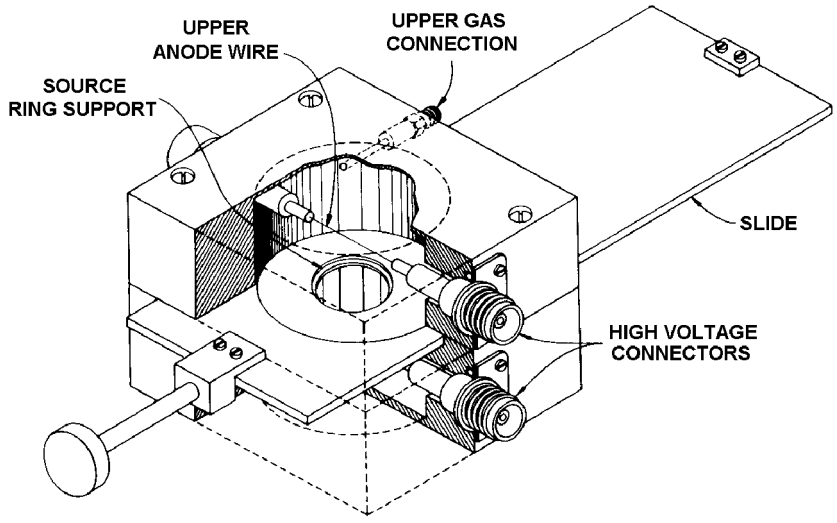


FIG. 8.10. A $4\pi$ proportional counter for measuring absolute decay rates. (Acc. to O'Kelley.)

Table 8.2. *Properties of some representative counter tubes*

| | Geiger–Müller counters | | Proportional counters | |
|---|---|---|---|---|
| Purpose | β, γ | α, β | n | α, β |
| Wall thickness | 0.1mm glass | 1.5 mg/cm$^2$ mica | 1 mm steel | 0.3 mg/cm$^2$ foil |
| Filling gas | Ne + Ar + halogen | Ar + organic | $BF_3$ enriched in $^{10}B$ | Pure $CH_4$ |
| Operating voltage | 700 V | 1250 V | 2200 V | α 1900, β 2600 V |
| Plateau length | > 250 V | ~300 V | > 300 V | α > 800 V, β~400V |
| Plateau slope | 8%/100 V | < 4%/100 V | < 2%/100 V | < 2%/100 V |
| Lifetime | $> 3 \times 10^9$counts | $3 \times 10^8$counts | | Infinite |
| Dead time | 140 μs | 300 μs | | 3 μs |
| Background count rate | 20–30 cpm | 80 cpm | 1–2 cpm | α 0.1 cpm<br>β 20–25 cpm |
| Background shielding | 50 cm Pb | 10 cm Pb | | 50 cm Pb |
| Special features | Insensitive to overvoltage | | Insensitive to γ | |

Another technique for neutron detection uses a *fission chamber*. One design contains a stack of alternate anodes and cathodes, one of the electrodes being covered by a thin layer of uranium enriched in $^{235}U$. The fission fragments produce large ionization even though the gas multiplication is quite low. This detector is more sensitive to fast neutrons than the $BF_3$ counter, and can be used for fast neutron fluxes up to ~ $10^{10}$ n m$^{-2}$ s$^{-1}$ with a background of a few cps.

### 8.3.3. *Geiger-Müller counters*

In region IV (Fig. 8.7), the proportionality between the primary ionization and the output pulse disappears and the latter becomes the same size for all initial ionization whether it be a 6 MeV α-particle or a 50 keV X-ray. Geiger-Müller (GM) counters which operate in this region have high sensitivity to all different kinds of radiation and the large size of the output pulse (from a tenth of a volt to one volt, compared to the several tenths of a millivolt output of ionization chambers) requires much less external amplification. This considerably reduces the complexity of the auxiliary electronic equipment. The detector tubes for GM counters are quite simple and allow a great deal of flexibility in design. Figure 8.8(a) shows a GM tube with a jacket for flowing liquids; Table 8.2 gives the properties of some other typical GM tubes. In general GM counters are limited to handling lower count rates than proportional counters.

As in the case of proportional counters, the primary electrons from the ionizing radiation cause secondary ionization near the center anode wire in GM detectors. This initial avalanche ends when the very mobile electrons are all collected by the anode. However, the neutralization of the electrons at the wire produces photons, which react with the gas leading to the emission of photoelectrons. These trigger further avalanches and an overall avalanche spreads along the complete length of the center wire and continues until the build-up of the positive ion sheath progresses to a point sufficient to reduce the field strength sufficiently to prevent further ionization. This build-up takes place because the

heavy positive ions have such a slow rate of movement that they are essentially stationary during the time interval of the electron avalanches. The time required to reach this point in the process is of the order of a few microseconds. Since the resolving time is of the order of 100 μs due to the slow movement of the heavy cations to the cathode, it is necessary to make coincidence corrections in GM counting at much lower count rates than in the case of proportional counting. Typically, corrections are significant for count rates exceeding 10 000 cpm.

When the positive ion sheath reaches near the cathode it may induce new avalanches as it collides with atoms in the gas and produces UV-light or emission of electrons. To avoid a recurring pulsing, which would render the counter useless, it is necessary to prevent further avalanches at this point by a process of quenching. This is usually accomplished by the addition of a small amount of an organic compound such as ethyl alcohol or ethyl formate or a halogen to the counting gas. Since the ionization potential of the organic molecule is lower than that of argon, the usual counting gas, when the positive argon sheath moves to the cathode and encounters organic molecules the following reaction occurs:

$$Ar^+ + C_2H_5OH \rightarrow Ar + C_2H_5OH^+$$

In this reaction the charge of the argon ion is transferred to the organic molecule which gains an electron upon striking the cathode. The energy acquired in the neutralization causes dissociation into uncharged fragments rather than producing photon or electron emission. Inasmuch as the quenching gas is dissociated in the process of counting, such GM tubes have limited lifetimes which usually amount to approximately $10^9$ discharges.

Chlorine and bromine have strong absorption bands below about 251 nm for the photons emitted, leading to dissociation. In the recombination the halogen molecule returns to its ground state via a series of low energy excited states. This makes halogens useful as quenchers in GM tubes. Halogen-filled GM tubes are popular because of their infinite lifetime and low operating voltage. Another advantage is that they will not be damaged by wrong polarity or excess voltage, as is the case with the organic quenched tubes.

GM tubes are available in a wide variety of shapes and sizes. Tubes have been used successfully which varied from approximately 1 mm to several centimeters in diameter and from 1 cm to almost a meter in length. The cathode can be made by coating the inside of a glass cylinder with a conducting material such as metal or graphite while the anode may be a tungsten wire mounted coaxially. The "end-window" GM tube has a thin mica window and the center wire is terminated with a glass bead. The cathode is always at ground potential while the anode is at a high positive potential.

When the radiation intensity is measured as a function of the electrode potential it is found for GM counters (as for proportional counters) that over a certain voltage interval there is little, if any, change in the measured count rate. This is known as the *plateau region* (Fig. 8.8). This is the voltage range in which the detectors are operated since they are relatively insensitive to small voltage changes in this region. For organic quenched GM tubes the plateau commonly occurs between 1200 and 1500 V and its slope should not exceed 5% per 100 V. Halogen-quenched tubes operate at a lower voltage but have higher plateau slopes (cf. Table 8.2).

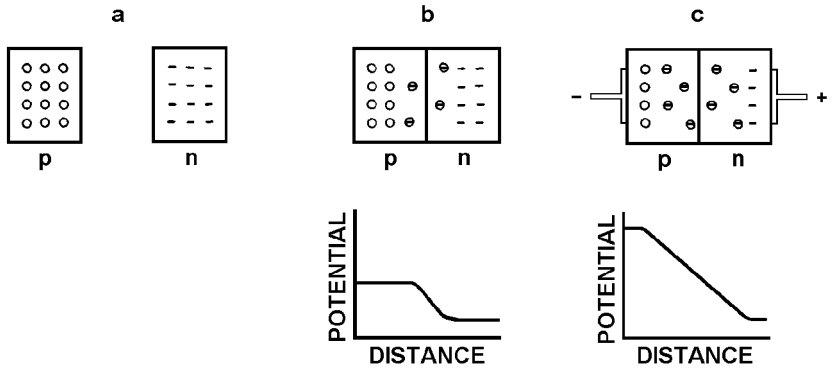


FIG. 8.11. Formation and properties of a p-n junction in a semiconductor.

### 8.4. Semiconductor detectors

The semiconductor detector is similar to an ordinary semiconductor diode composed of p-type and n-type semiconductor material. This detector has become dominant for nuclear spectroscopy (i.e. determination of the energy of nuclear radiation) but it is not so often used for simple measurement of count rates.

Semiconductors are materials like silicon (resistivity ~ $10^3$ Ωm) and germanium (0.6 Ωm) with resistivities between metals (e.g. copper, $10^{-8}$ Ωm) and insulators (e.g. quartz, $10^{12}$ Ωm). A crystal of pure silicon placed between two electrodes is almost nonconducting. The electrons in the material are almost all *valence electrons*, bound to specific silicon atoms with an energy of 1.115 eV at room temperature (0.75 eV for Ge at 80 K). If 1.115 eV is given to an electron in silicon, it moves to a band of overlapping energy levels which are not associated with specific atoms. The electron moves readily through the crystal in this "conduction band", i.e. the crystal conducts electricity. At a certain temperature some electrons, according to the Maxwell energy distribution, always have the necessary energy to be in the conduction band. These electrons provide a very small conductivity for pure silicon; this is referred to as the *intrinsic conductivity*. For diamond, the gap between the valence and conducting band is 7 eV, which is so large that essentially no electrons are found in the conduction band at room temperature, and thus diamond is an insulator.

The energy needed for transferring valence electrons to the conduction band can be supplied by nuclear radiation. The average energy needed to produce an electron-hole pair in silicon at room temperature is not 1.115 eV but 3.62 eV because some energy is lost as crystal excitation (3.72 eV in Si and 2.95 eV in Ge at 80 K). The electron removed from the valence band leaves a vacancy or "hole". The ionization is said to give an *electron-hole pair*. Just as the electrons move towards the anode, the holes move towards the anode.

Si has 4 valence electrons while P has 5 and In 3. If we introduce a very small amount of phosphorus into silicon, the phosphorus atoms substitute for silicon in the crystal lattice. Each such phosphorus has an excess of 1 electron. These electrons are not free but are very weakly bound, such that only 0.04 eV is needed to transfer them into the conduction bands. Because phosphorus donates extra electrons to the system, it is referred to as a *donor material*. Silicon which contains small amounts of donor material (usually referred to as

"impurity") is called *n-type silicon* since it has excess negative charge and conduction is by electrons.

If instead, indium is the impurity in the silicon crystal structure, the opposite effect is produced. Such material contains a number of energy levels only 0.06 eV above the valence band; the result is holes in the valence bands. Such material is referred to as *acceptor material*. Silicon with acceptor material is called *p-type silicon*, since the holes are considered to be positively charged. Conduction is in this case by movement of holes. The addition of controlled amounts of impurity atoms thus provide *charge carriers* (as the electrons and holes collectively are called, c.f. §8.2) and produces the desired properties in semiconductor materials.

The most interesting effect comes from the combination of two types of silicon, one n-type and another p-type (Fig. 8.11(b)). The contact surface is referred to as a *p-n junction*. At such a junction some positive holes move to the n-type material, and vice versa. As a result a "depletion" layer a few microns thick is established at the junction where all the holes are filled with electrons and the layer is depleted of charge carriers. A p-n junction can be produced in a single piece of silicon by doping it with the proper impurity from either side of the crystal and by other techniques like ion implantation.

If a voltage is applied over the junction by connecting the negative terminal to the p-type region and the positive terminal to the n-type region, the junction is said to be *reversely biased*. With such reverse bias, the barrier height and depletion layer thickness increase. As a result the crystal opposes any current as the resistivity becomes very high. In the reverse direction the semiconductor represents a high resistance shunted by a capacitive component (Fig. 8.3(a)) due to the dielectric of the barrier layer (the p-n junction diode).

A number or variations of this basic design exist. The point of importance for semiconductors as nuclear detectors is that a depleted layer with a high space charge is formed. A nuclear particle entering this volume forms electron-hole pairs, which are rapidly and efficiently collected at the electrodes due to the high potential gradient. By this a charge is transported through the crystal while the original conditions are restored.

There are some formal similarities between the function of a semiconductor detector and a parallel plate ion chamber. In comparison with ionization chambers the semiconductor detector (i) requires only 3.62 eV (Si, 300 K) or 2.95 eV (Ge, 80 K) for an electron-hole pair (as compared to about 15 – 35 eV for an ion pair in a gas), (ii) collects the charge much faster (no slow positive ions), (iii) has a much higher stopping power, (iv) but does not normally have the property of charge multiplication. The charge through the semiconductor detector is given by (8.2) where $\eta$ (the collection efficiency) is usually very close to 1, and $w$ is 3.62 eV for silicon at 300 K and 2.95 eV for germanium at 80 K. It is seen that the signal is directly proportional to the energy absorbed in the detector as long as $\eta$ is constant. Because $w$ is much smaller in semiconductor detectors than in gas and scintillation detectors, more primary electrons are released in each absorption event, which gives better "statistics" (see §8.11) and higher energy resolution. This makes semiconductor detectors useful for nuclear spectroscopy, although for $\alpha$- and $\beta$-spectroscopy the precision is higher with magnetic deflecting devices (cf. §2.3).

### 8.4.1. *Surface barrier detectors*

The surface barrier detector is a p-n type silicon diode wafer characterized by a rather thin depletion layer (Fig. 8.12(a)). It is made of n-type silicon on which one surface has been etched prior to coating with a thin layer of gold (typically ~40 μg/cm$^2$) and the other surface coated with a thin layer of aluminum (typically ~40 μg/cm$^2$) to provide electrical contact. This results in a window-layer which is equivalent to ~800 Å of Si. Depending on the applied voltage, the detector can be partially depleted (inactive entrance layer), totally depleted (no inactive layer), or overdepleted (higher applied potential than required for total depletion). Surface barrier detectors are used mainly for α- and β-spectroscopy and for d$E$/d$x$ and $E$ measurements for high energy particles, although the efficiency is limited by the sensitive surface diameter (≤ 10 cm) and the energy range by depleted layer thickness (≤ 5 mm).

The radiation sensitive depleted layer is available in various thicknesses, ≤ 5 mm, enough to stop electrons of ≤ 2.2 MeV, p of ≤ 32 MeV, and α of ≤ 120 MeV. A typical silicon surface barrier detector for α-spectroscopy has a sensitive area of 300 mm$^2$, 300 μm depletion depth, 20 keV FWHM (full width at half maximum) and operates at 100 V reverse bias. The resolving time is about $10^{-8}$ s. Special "rugged" detectors are available which have an acid resistant $SiO_2$ surface layer permitting cleaning and contact with liquids. Detailed information for detector selection is available from various detector manufacturers.

When used for α- or β-spectroscopy, a vacuum is applied between the detector and the radiation source. In the absence of a vacuum for α-radiation the energy loss is about 1 keV per 0.001 atm per cm distance between source and detector. The absorption in the detector window for a 6 MeV α is less than 6 keV. A resolution of about 12 keV FWHM can be obtained for a 6 MeV α, Figure 8.11.

In totally depleted silicon surface barrier detectors the sensitive region extends through the whole thickness of the silicon, which may be in the form of a very thin slice (e.g. 20 μm). A particle passing through such a detector loses a small fraction of its energy d$E$/d$x$ and may then be completely stopped in a second (much thicker depleted layer) detector to lose the remainder of its energy, which may essentially be its original total $E_{kin}$. Particle mass $A$ and charge $Z$ can be determined from d$E$/d$x$ and $E$, e.g. with the aid of the proportionality

$$E\,\mathrm{d}E/\mathrm{d}x \propto A\,Z^2 \tag{8.13}$$

Figure 8.13 shows a hypothetical distribution when the recorded intensities of $^1$H, $^2$H,and $^3$H are plotted against $E$ d$E$/d$x$.

High energy particles not only cause ionization in the detector crystal but may displace some detector atoms from the crystal lattice. Radiation damage decreases with applied bias and increases with the particle mass. Such radiation damage to the crystals limits the lifetime of the detectors. The threshold dose (in particles/cm$^2$) is about $10^8$ for fission fragments, $10^9$ for α, $10^{10}$ for $p^+$, $10^{12}$ for fast neutrons, and $10^{13}$ for $e^-$. Radiation damage can usually be removed if the detector can be annealed at 200°C.

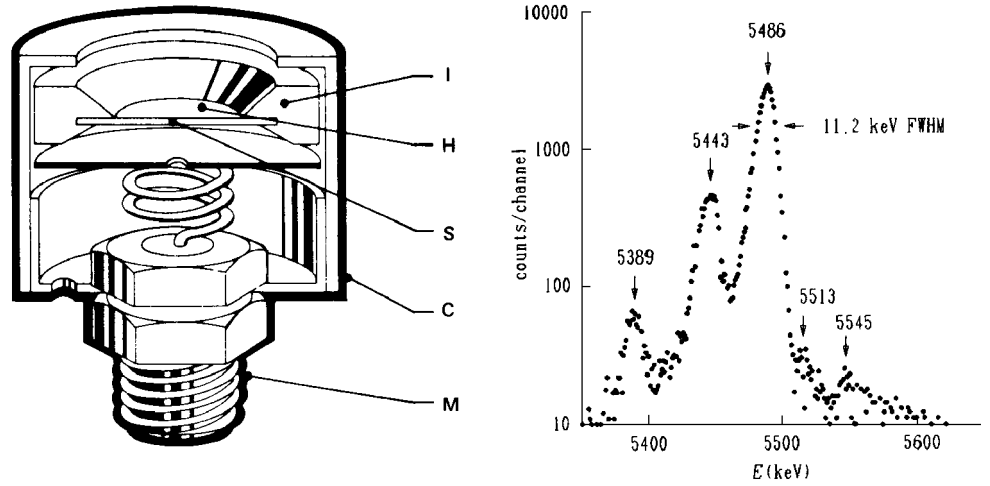


FIG. 8.12. (a) Surface barrier detector; S detector wafer, H gold surface layer, M connector. (b) α-spectrum of $^{241}$Am measured with a high resolution detector (Acc. to ORTEC.)

### 8.4.2. *Lithium-drifted detectors*

The probability of γ-interaction is so small in the small depletion depth of the surface barrier detectors that they are not very useful for γ-spectroscopy. Large depleted volumes can be created by drifting lithium atoms into a silicon or germanium crystal. Lithium does not occupy a crystal site in the crystal, but is small enough to go into interstitial sites. The ease of ionization of Li to $Li^+$ makes it a donor impurity. The lithium is drifted from one side of the crystal using an electric field. Its concentration at the "entrance" side becomes high and then decreases towards the other end of the crystal. The amount of lithium in the

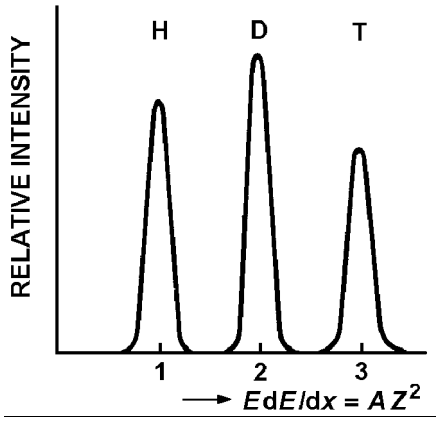


FIG. 8.13. Plot of relative particle intensities for H, D, and T versus $EdE/dx$ in a two-detector telescope, where the first detector records $dE/dx$ and the second $E$.

crystal adjusts itself during the drifting process so that the lithium atoms compensate the impurities. This is, however, not a stable situation when the drifting operation is stopped. Hence, the final state is "frozen" by cooling of the drifted crystal to liquid nitrogen temperature. Accidental heat-up will destroy the lithium compensation and the detector must be redrifted.

When a potential is applied over such a crystal, with the positive terminal at the high lithium side, three volumes are created, one of p-type, a middle "intrinsic" one, and an n-type one (p-i-n detectors). In the intrinsic volume the lithium donor electrons neutralize any original impurities, which are of acceptor p-type. The intrinsic volume becomes depleted and thereby sensitive to nuclear radiation, and detectors with depleted volumes up to more than 100 $cm^3$ are commercially available. Figure 8.14 shows the arrangement of the Dewar vessel with liquid $N_2$, cold-finger, detector, and preamplifier.

Lithium-drifted detectors are made either from silicon (Si(Li) detectors) or from germanium (Ge(Li) detectors). The latter has a higher atomic number and density than silicon and is therefore preferable for γ-spectrometry. For 60 keV X-rays, the efficiency of a Si(Li) detector may be 5%, while for a comparable Ge(Li) detector it may be 100%. At lower energy the Si(Li) detector is preferable, especially if the measurements are carried out in a high γ-background. Si(Li) detectors are of particular importance in X-ray fluorescence analysis (cf. §6.8.4).

Both types give excellent resolution, for a good Si(Li) X-ray detector about 160 eV at 5.9 keV and for a good Ge(Li) detector about 1.75 keV FWHM for 1.33 MeV γ. Energy resolution of Ge detectors varies with energy below 1.5 MeV according to the empirical

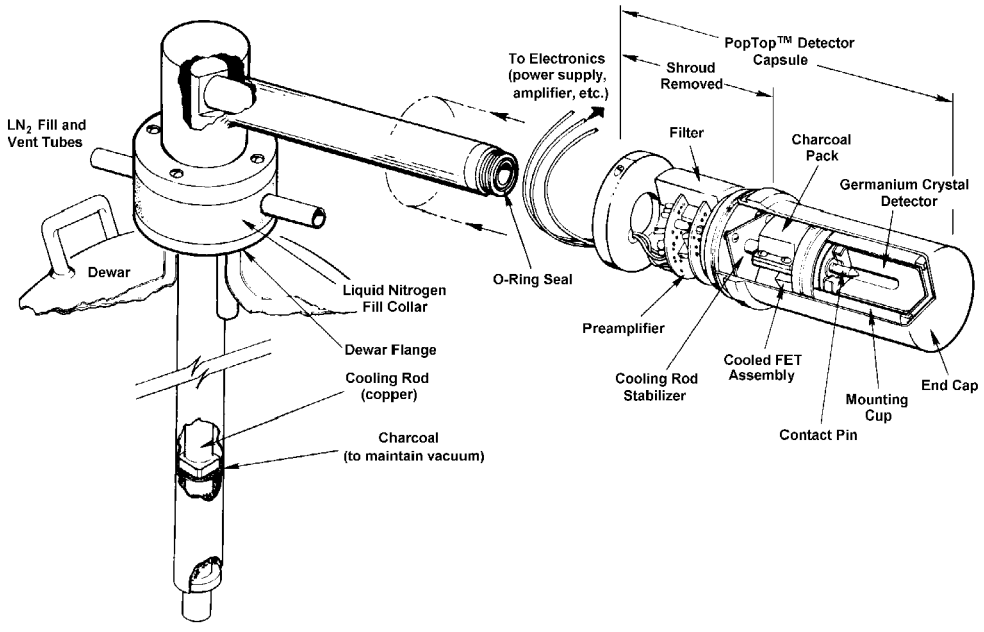


FIG. 8.14. Cut-away view of a Ge-detector showing Dewar, cold-finger, preamplifier and germanium crystal. (Acc. to ORTEC.)

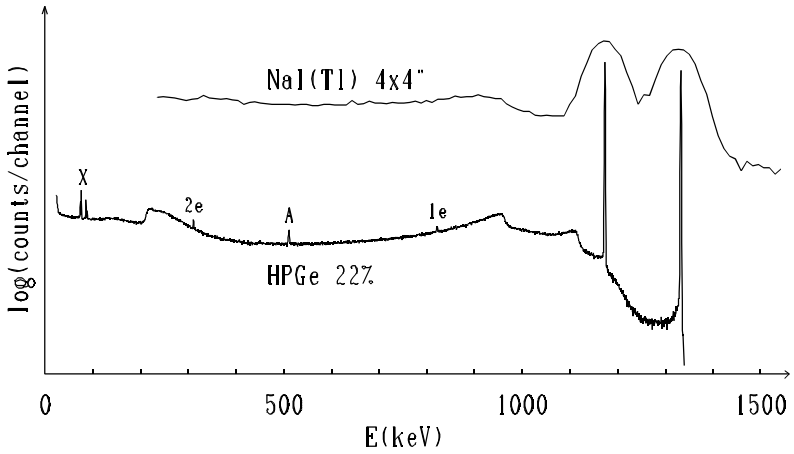


FIG. 8.15. Energy spectrum of $^{60}$Co obtained with scintillation and HPGe detectors.

eqn. FWHM $\approx (n^2 + kE_\gamma)^{1/2}$, where FWHM is the full peak width at half maximum, $n$ the noise line width, $k = 2$, and $E$ γ-energy, all in eV units. This resolution is far superior to that of the scintillation detector, as is seen from Figure 8.15. On the other hand, the detection efficiency is usually smaller. However, an efficiency higher than 100% of that obtained with a 3" × 3" NaI(Tl) scintillation detector for 1.33 MeV γ-rays (which is the reference for Ge-detector efficiency) has been obtained in the best designs, but typical values are 10 – 30%.

### 8.4.3. *Intrinsic detectors*

One reason for drifting lithium into silicon and germanium is the necessity to compensate some p-type (acceptor) impurities normally present in pure materials. It is now possible to increase the purity of germanium to 1:$10^{13}$ (compared to earlier 1:$10^{11}$) Which makes lithium-drifting unnecessary. In addition, these intrinsic germanium detectors make uninterrupted cooling less important; it is not required when storing the crystals, but should be used when measuring in order to improve resolution and prevent crystal overheating. Depending on the type of dominating impurity, HPGe crystals can be of either n- or p-type. HPGe-detectors of p-type have usually a lower energy cutoff, beginning at about 100 keV, caused by the detector capsule wall and insensitive entrance layer. Commercially available p-type detectors have relative efficiencies of 10 – 100%. On the other hand n-type HPGe-detectors can be made with a very thin entrance layer and, when fitted with a Be-window, have a low energy cutoff beginning at about 6 keV. Relative efficiencies for n-type HPGe detectors are in general somewhat less than for p-type detectors, i.e. 10 – 80%. Intrinsic germanium detectors are to a large extent replacing the lithium-drifted germanium detectors because of their greater handling simplicity at no higher cost or loss of resolution.

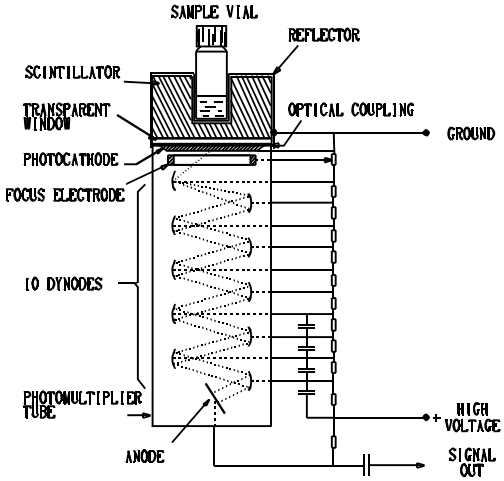


FIG. 8.16. Well-type scintillation detector with photomultiplier circuitry.

## 8.5. Scintillation detectors

In 1908 Rutherford and Geiger established the reliability of a method of counting α-particles by observing visually the flashes of luminescence[1] produced in a thin layer of ZnS by the α-particles. Since the development of reliable *photomultiplier* tubes (PMT) in 1946, scintillating counting techniques have played an important role in nuclear science. A scintillation detector consists of a *scintillator*, or *phosphor* optically coupled to a PMT which produces a pulse of electric current when light is transmitted to the tube from the scintillator (see Fig. 8.16). The scintillating material can be an inorganic crystal or an organic solid, liquid, or gas. Detectors with sandwiched scintillators of different kind, phoswich-detectors, can, with suitable electronics, use the difference in scintillator properties (light output and decay time), thickness and position in the sandwich to differentiate between radiation types and radiation energies permitting e.g. simultaneous separate counting of α- and β,γ-radiation.

In organic substances the absorbtion of energy raises the organic molecule to one of the vibrational levels of an excited electronic state (see §§7.5 and 7.8). Through lattice vibrations some of the excitation energy is dissipated as heat and the molecule decays to lower vibrational levels of the exited electronic state. After approximately $10^{-8}$ s, a time sufficient for many molecular vibrations, the molecule may return to the ground electronic state with emission of light photons. Since the energy which excites the molecule is in general larger than that emitted in any single step in the decay back to the ground state, reabsorption of these emitted photons is unlikely, and the crystal is consequently transparent to the emitted photon. This transparency is necessary if the scintillations are to escape the scintillator and reach the PMT. Aromatic hydrocarbons such as anthracene and stilbene which have resonance structures are excellent scintillators. Liquid and solid solutions of such organic substances as p-terphenyl are also used as scintillators. In these systems the

[1] *Luminescence* includes both fluorescence and phosphorescence (§§7.5 and 7.8).

Table 8.3. *Properties of some common phosphors*

| Material | Density (g cm$^{-3}$) | Wavelength of maximum emission (nm) | Decay constant for emission (μs) | Relative pulse height |
|---|---|---|---|---|
| Gaseous | | | | |
| Xe | n.a. | 325 | small | 9[b] |
| Kr | n.a. | 318 | small | 5[b] |
| Inorganic | | | | |
| NaI(Tl)[a] | 3.67 | 410 | 0.23 | 100[c] |
| CsI(Na) | 4.51 | 420 | 0.63 | 85[c] |
| CsI(Tl) | 4.51 | 565 | 1.0 | 45[c] |
| ZnS(Ag) | 4.09 | 450 | 0.20 | 130[b] |
| $CaF_2$(Eu) | 3.19 | 435 | 0.9 | 50[c] |
| Organic | | | | |
| Anthracene | 1.25 | 440 | 0.032 | 100[d] |
| Stilbene | 1.16 | 410 | 0.006 | 60[d] |
| Plastic phosphors | 1.06 | 350-450 | 0.003-0.005 | 28-48[d] |
| Liquid phosphors | 0.86 | 355-450 | 0.002-0.008 | 27-49[d] |

[a](Tl), (Na), (Ag) and (Eu) indicate small amounts of these elements added as activators.
[b]For α-particles; NaI(Tl) = 100. [c]For γ-radiation; NaI(Tl) = 100. [d]For β-particles; Anthracene = 100.

energy absorbed through the interaction of radiation with the solvent molecules is transferred rapidly by the latter to the solute which undergoes excitation and fluorescence as described above. The exact mechanism of the transfer of energy from solvent to solute is not fully understood.

It is necessary to have small amounts of impurities in inorganic crystals to have luminescence. In ionic crystals in the ground state all the electrons lie in a lower valence band of energy. Excitation promotes the electrons into a higher conduction band of energy.

Table 8.4. *Quenching ratios for organic and aqueous solutions relative to water. Each sample contains 0.2 ml sample, 4 ml scintillator cocktail (Beckman Ready Solv CP) and 5 μl $^{147}$Pm solution.*

| Sample solution | Concentration | Quenching ratio (cpm/cpm$_{aq}$) |
|---|---|---|
| 1,2-Dichloroethane | 100% | 0.96 |
| Carbon tetrachloride | 100% | 0.06 |
| n-Hexane | 100% | 1.01 |
| Acetylacetone | 100% | 0.16 |
| Acetylacetone in n-Hexane | 0.1 M | 0.97 |
| MIBK | 100% | 0.82 |
| MIBK in n-Hexane | 0.1 M | 1.01 |
| Benzoylacetone in n-Hexane | 0.1 M | 0.90 |
| HTTA in n-Hexane | 0.1 M | 0.49 |
| Nitric acid | 1 M | 0.87 |
| Sulfuric acid | 1 M | 0.89 |
| Hydrochloric acid | 1 M | 0.93 |

If impurities are present they can create energy levels between the valence and conduction bands, as described in §8.4. Following excitation to the conduction band through absorption of energy an electron may move through the conduction band until it reaches an impurity site. At this point it can "decay" to one of the impurity electron levels. The de-excitation from this level back to the valence band may occur through phosphorescent photon emission. Again, since this photon would have an energy smaller than the difference between the valence and conduction bands, these crystals are transparent to their own radiation.

To be useful as a scintillator a substance must possess certain properties. First, there must be a reasonable probability of absorption of the incident energy. The high density in solid and liquid scintillators meets this condition. Following absorption, emission of luminescence radiation must occur with a high efficiency and – as mentioned – the scintillator must be transparent to its own radiations. Finally, these radiations must have a wavelength that falls within the spectral region to which the PMT is sensitive. Since this is not always the case, particularly with liquid scintillators, "wave-length shifters" are added (e.g. diphenyl-oxazolbenzene (POPOP) to solutions of p-terphenyl in xylene). Further, "quenching" substances which absorb the light emitted from the scintillator should be absent. This is a particular problem in liquid scintillation counting.

Table 8.3 lists the properties of some common scintillators. The data indicate that the greater density of inorganic crystals makes them preferable for γ-ray counting. The resolving time is shorter for the organic systems whether liquid or solid. When large detector volumes are necessary a liquid solution system is the simplest and most economical.

The scintillator must be coupled optically to the PMT so that there is a high efficiency of transfer of the light photons to the PMT photo cathode. Since PMTs are sensitive to light in the visible wavelength region, both scintillator and PMT must be protected from visible light. Figure 8.16 shows a typical combination of a "well-type" crystal phosphor and PMT. The light sensitive photo cathode of the PMT is a semitransparent layer of a material such as $Cs_3Sb$ which emits electrons when struck by visible light. The emitted photoelectrons are accelerated through a series of 10-14 electrodes (*dynodes*) between which a constant voltage difference is maintained. When the photoelectrons strike the nearest dynode, secondary electrons are emitted as the dynodes are also covered with $Cs_3Sb$. Consequently, there is a multiplication of electrons at each dynode stage and at the last dynode the number of original electrons have been increased by about a factor of $10^6$ over a total voltage drop in the photo tube of 1000 – 2000 V. The electrical signal is normally generated from a voltage change between ground and the anode caused by a resistor between anode and bias supply.

### 8.5.1. *Gas scintillator detectors*

Several high purity gases are useful scintillators, notably $N_2$, He, Ar, Kr and Xe. Except for $N_2$, much of the emitted light lies in the UV range. Hence, PMTs sensitive to UV must be used or a wave-length shifting gas like $N_2$ added. The scintillations produced are of very short duration, a few ns or less, which puts them among the fastest of radiation detectors. Gas scintillators have easily variable size, shape and stopping power. The latter by changing the gas pressure. They are often unusually linear over a wide range of particle energy and

d*E*/d*x*. However, the light yield is, at best, an order of magnitude lower than that of NaI(Tl). This has mostly limited their use to counting of α and other energetic multiply charged particles. Gas-flow detectors are discussed in §8.8.

### 8.5.2. *Liquid scintillator detectors*

Liquid scintillators have a wide use for routine measurement of β-emitters, particularly low-energy ones like $^{3}$H and $^{14}$C, in liquid samples, especially in biochemistry and in hospitals. Since these isotopes are very important in biochemical applications, most of the development of liquid scintillation technique has been focused on them.

The sample is directly dissolved in the liquid scintillator solution (*scintillator cocktail)* and the light output measured by PMTs. Normally two PMTs are used in order to eliminate much of their internal noise by only accepting coincident pulses from both tubes. Liquid scintillation counting offers several advantages when measuring low-energy β-emitters compared to most other detectors. Problems like attenuation by the detector window, self-absorption and backscattering are avoided. However, the introduction of the sample into the scintillator medium often reduces the light output considerably, see Table 8.4 and Figure 8.17. This effect is called *quenching* and depends on phenomena such as chemical reactions that absorb some of the deposited energy (*chemical quenching*) and changes in optical properties (*color quenching*). A reduction in light output reduces the efficiency, especially at low β-energies. For low quenched samples the efficiency may approach 100% since the β-particles almost always have to encounter the scintillator. The energy resolution is sufficiently good to differentiate between e.g. $^{3}$H ($E_{\beta,\max}$ 18 keV) and $^{14}$C ($E_{\beta,\max}$ 160 keV).

Measurement of α-emitters is also feasible. In this case several MeV of energy is deposited in the scintillation cocktail, usually yielding near 100% detection efficiency. The high amount of energy deposited also reduces sensitivity to quenching. The energy resolution for α-particles is at best 5 – 10% and thus far inferior to that of surface barrier detectors. By means of special electronics the difference in light-pulse decay time between scintillations caused by α (long decay time) and by β,γ (short decay time) can be used to measure α-emitters in samples with a high β,γ-background. Liquid-flow detectors are discussed in §8.8.

### 8.5.3. *Solid scintillator detectors*

ZnS(Ag) is a traditional phosphor for α-detection while anthracene and stilbene can be used for β-particle detection. For γ-rays, sodium iodide with a small amount of thallium impurity, NaI(Tl), is the most common phosphor. CsI(Tl) is another often used scintillator because it can be formed to special shapes, e.g. thin sheets, much easier than NaI(Tl). Plastics with incorporated organic scintillators are often used in nuclear physics experiments because they produce short light pulses and can be made in various shapes.

Detectors with scintillation crystals are used commonly for routine radioactivity measurements, particularly of γ-emitters, because of their reliability. As compared to GM tubes they have the advantage of shorter resolution time and higher γ-efficiency, although they require a more stable high voltage supply. Particularly the well-type crystal shown in

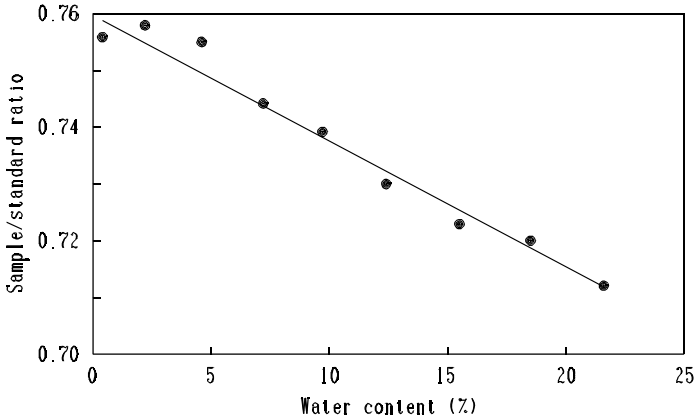


FIG. 8.17. Quenching effect of water. The sample/standards ratio is the count rate ratio between 4 ml scintillator cocktail (Beckman Ready-Solv HP) + water and Packard reference standard.

Figure 8.16 is popular because of the high counting efficiency for samples introduced into the well ($\psi \geq 0.9$). For counting very large liquid volumes (e.g. environmental, water samples) a specially designed sample vessel is used which fits over and around the cylindrical detector arrangement (Marinelli beaker).

### 8.6. Cerenkov detectors

The Cerenkov effect described in §6.4.3 can be used for detection of high energy β-radiation because the velocity of the nuclear particle must exceed the ratio $\mathbf{c}/n$, where $n$ is the refractive index of the absorber.

$$E_{\beta\text{threshold}} = 0.511\,[-1 + \{1 + (n^2 - 1)^{-1}\}^{1/2}] \text{ (MeV)} \qquad (8.14)$$

The β-threshold energy in lucite ($n = 1.5$) is 0.17 MeV, so lucite and similar plastics are often used as particle absorbers in Cerenkov detectors. In order to detect the light emitted, PMTs are placed in the direction of the emitted light. There are many similarities between scintillation and Cerenkov detectors; however, the light pulse from the Cerenkov detector is faster, $\sim 10^{-10}$ s, but smaller than from scintillation detectors. The advantage of the Cerenkov detector is that aqueous or organic (uncolored) solutions can be used without the need to add a scintillator, that soft β-emitters and γ-emitters give little or no signal, and that the angle of emitted light reveals the velocity of the absorbed particles. At energies $< 10$ MeV, only β-particles are detected.

## 8.7. Electronics for pulse counting

A wide variety of counting systems has been developed for various purposes. Equipment is often built as NIM (Nuclear Instrument Module standard) or CAMAC (Computer Automated Measurement And Control standard) modules, which fit into standard bins (or crates) containing power supplies and some inter-module connections. Cable connectors are also largely standardized. This facilitates combinations of bias supplies, amplifiers, discriminators, SCAs, ADCs, counters, and other circuitry to fit any need as well as their connection to computers. Some non-standard units, e.g. portable instruments, have their own power supply, main amplifier, counter or rate-meter, etc.

### 8.7.1. *Preamplifiers*

The purpose of a preamplifier may be twofold. First of all it should increase the energy in the detector signal to such a level that it can drive a reasonable length of low impedance coaxial cable properly terminated at the other end with only a small loss in pulse amplitude. When the detector produces a very weak signal it may be advantageous to amplify that signal to a level where external noise becomes negligible. However, in some applications the detector signal is already large enough, the detector capacitance constant (e.g. a PMT) and *voltage sensitive preamplifiers* with unit gain are used, Figure 8.18(a).

A 0.5 MeV γ absorbed in a germanium crystal will only produce a charge of $2.7 \times 10^{-14}$ C (8.2). Moreover, the detector capacitance may change with operating conditions which make voltage sensitive preamplifiers less suitable and charge sensitive preamplifiers are preferred. The weak charge signal has to be integrated and converted to a voltage pulse by the preamplifier without adding too much noise. Figure 8.18(b) shows a typical input stage for a preamplifier used with germanium γ-ray detectors. The function of this stage is to integrate the total charge of the pulse through the detector converting it to a voltage signal with an amplitude that is proportional to the energy deposited in the detector. Often the input FET (Field Effect Transistor) of the preamplifier and the feedback resistor ($R_f$) are cooled to reduce their contribution to system noise. The charge accumulated on the FET

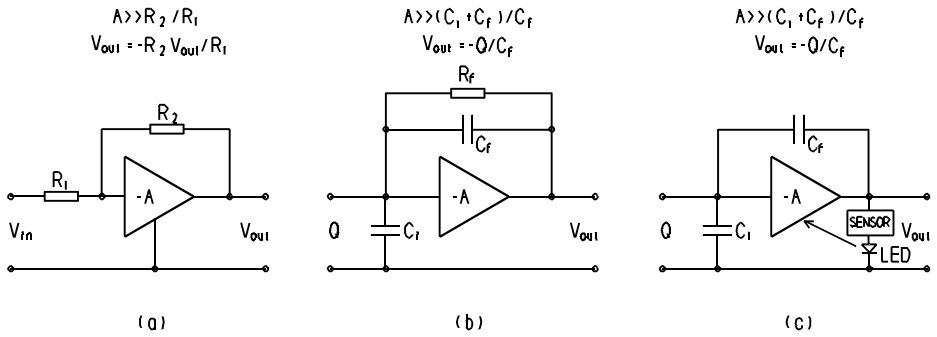


FIG. 8.18. Voltage sensitive (a), charge sensitive resistive feedback (b), and pulsed optical feedback (c) preamplifiers. A is amplifier gain.

is removed through a resistor - capacitor network, $R_f$ and $C_f$ in Figure 8.18(b), which is part of the amplifier feedback loop. This arrangement is called a *resistor feedback preamplifier*. The feedback resistor adds its inherent Johnson noise to system noise; typically 300 eV in FWHM with a resistor at room temperature. The contribution to the total noise level is, at least for a cooled resistor and FET, negligible in normal γ-spectrometry. However, when measuring low energy X-rays with a Si(Li) detector it may be important to reduce the noise further.

In the *pulsed optical feedback preamplifier*, Figure 8.18(c), the resistor is omitted and the input FET is permitted to charge-up in steps by each new pulse. The output signal is in the form of a staircase function and this is transformed to voltage pulses by differentiating circuits in the main amplifier. When the accumulated charge becomes too large (i.e. the output voltage is near its highest possible value) the sensor circuit triggers and the FET is irradiated with a short light pulse from the built-in light emitting diode thereby causing a short circuit in the FET, removing the accumulated charge. The reset operation produces a large voltage swing at the preamplifier output which may easily overload the main amplifier and make it distort pulses rapidly following the reset pulse. In order to avoid making measurements during and immediately after the big reset pulse a blocking signal is often available from the preamplifier during the reset pulse. A typical pulsed optical feedback preamplifier can, with a Si(Li) X-ray detector, give a FWHM of $< 150$ eV at 5.9 keV. The good resolution is important in low energy applications, e.g. X-ray measurements. A minor drawback of pulsed optical feedback is the extra dead time introduced by blocking measurements during each reset operation.

The output from a voltage sensitive or resistor feedback preamplifier is a tail pulse with a rather long decay time. Hence, some pulse pile-up is unavoidable, except at very low count rates. Pile-up will cause the average level of this signal to increase with pulse rate, which may approach the limit of linear operation of the preamplifier.

### 8.7.2. *Amplifiers*

The purpose of an amplifier to amplify a voltage pulse in a linear fashion and to shape the pulse so that the event can be analyzed easily and correctly in a short time. A linear amplifier accepts tail pulses as input, usually of either polarity, and produces a shaped and amplified pulse with standard polarity and amplitude span (NIM standard is positive polarity and 0 – 10 V amplitude). On most commercial linear amplifiers, the time constants for the various pulse shaping circuits are adjustable to fit various detector and count-rate requirements.

Biased amplifiers shifts the zero of the amplified pulse down while still producing only positive output pulses. This effect is important in e.g. α-spectrometry as the lower energy range is normally of no interest and it is better to use the available output amplitude span to enlarge the interesting energy region than to cover the whole energy range.

Amplifiers with a logarithmic response have use in liquid scintillation counting for compression of the higher energy part of the β-spectrum.

### 8.7.3. *Single channel analyzers*

The pulse obtained from many detectors is directly proportional to the energy absorbed in the detector. If all of the energy of the nuclear particle is absorbed in the detector, which is possible for all kinds of ionizing radiation, and only one particle or photon interacts at a time with the detector, the energy of the particle or photon can be determined from the size of the generated pulse. In single-channel analyzers (SCA) only one channel exists which serves as a "window" to accept only pulses of a certain size corresponding to a limited range of energy as indicated in Figure 8.5(b). This window can be moved in steps through the entire energy range, thereby obtaining a measure of the count rate of particles having different energies. In the figure the window position and width are set so as to cover only the middle peak. By narrowing the window, and moving it from zero to maximum pulse amplitude, the whole particle energy spectrum is obtained. Spectrometry represents one of the principal techniques whereby the energy of ionizing radiation is measured. The single channel spectrometer is a system for energy determinations, although multichannel systems are simpler to use, more accurate and faster.

The main use of SCAs is to select events within a given energy interval. Thereby the background count rate is very much reduced which increases sensitivity. One of the most important routine uses of SCAs is in simultaneous $^{3}H$ and $^{14}C$ counting using liquid scintillators. Two SCAs are normally used, one set to cover pulses corresponding to the very soft $\beta^-$ from $^{3}H$ and the other set to cover the more energetic pulses caused by the $\beta^-$ from $^{14}C$.

### 8.7.4. *Counters and rate meters*

Ultimately the amplified pulses must often be accumulated over a fixed time interval and the resulting number displayed. The device used is based on a simple electronic register which is incremented by one each time a pulse arrives at its input. Such devices are often called *counters* or *scalers*. Counters can usually be operated in two modes, *preset time* or *preset count*. Counting is started and stopped by manual push buttons or by logic signals from other units, e.g. the logic stop signal from a timer in the preset time mode. In the preset count mode, the scaler stops at a given count and produces a logic output signal which can be used by other units, e.g. to stop a timer.

In some applications a continuous display or record of the count rate is desired, e.g. in a survey meter. This is achieved by use of a *count rate meter*. Count rate meters can be analog (based on a diode pump) or digital (based on a recycling scaler-timer-display unit). In either case, the value obtained follows the input rate with a certain time-lag, determined by the *time constant* used. A high time constant gives a smooth reading as it averages input pulse rate fluctuations over a longer time interval, but a very sluggish response to true input rate changes. Correspondingly a short time constant gives a rapid response but also a very fluctuating reading.

### 8.7.5. *Multichannel analyzers*

Multichannel analyzers (MCA) consisting of an analog to digital converter (ADC), controller and storage unit which may have 16 000 channels or more (i.e. the energy scale is split up into that number of steps). In this case the pulses are sorted immediately into the various channels which record the counts as they occur rather than scan over an energy range in steps. In many designs the MCA is interfaced to a computer to provide display, recording and analysis of the energy spectrum. MCAs are also made as circuit boards that fit inside a personal computer and have suitable software by which the PC can emulate a stand-alone dedicated MCA. The ADC unit is normally based on one of two principles.

In a Wilkinson ADC, the beginning of an input pulse starts a pulser (the clock) and a ramp voltage. When the input signal culminates its amplitude is "frozen" by a sample-and-hold gate. The pulser runs until the ramp voltage crosses the frozen input signal level. By accumulating the pulser signals in a counter the final count is proportional to the amplitude of the input pulse. This count can then be used as a digital address, *channel*, telling the attached digital circuitry where to increment the stored counts. The dead time of this ADC type is roughly proportional to the amplitude of the input pulse and to the highest address permitted. A typical conversion time with a 100 MHz clock may be $1 + 0.01\,n$ μs, for channel $n$. Wilkinson ADCs are mostly used in MCAs with a relatively small number of channels.

The successive approximation ADC locks the maximum amplitude in a sample-and-hold circuit and uses an ultra fast digital voltmeter of successive approximation type to measure the amplitude. A typical conversion time is ~ 25 μs at 4000 channels full scale. The voltmeter reading is then used as address in the same way as for the Wilkinson ADC. This type of ADC has usually a fixed dead time, independent of the pulse amplitude and only moderately dependent on the maximum address (each doubling of the number of channels adds the same increment to the conversion time). Successive approximation ADCs are preferred for MCAs with very many channels as they then, on the average, become faster than Wilkinson ADCs. On the other hand the linearity of a Wilkinson ADC is usually slightly better than for a successive approximation ADC.

MCAs are probably the most versatile instruments for nuclear particle detection because of their usefulness both for qualitative identification and quantitative determination of radioactive nuclei. Practically all α- and γ-spectra reproduced in this book have been obtained through this technique.

In case correlated events registered by several ADCs are measured the addresses from the ADCs and time is usually recorded digitally on a magnetic storage medium in real time. The desired information, e.g. γ–γ coincidences, is then obtained by reading and sorting the stored data after the experiment.

### 8.7.6. γ-*spectrometry*

As we learned in §6.5, the capture of a γ-ray in an absorber such as a NaI(Tl)- or Ge-crystal occur by any of three processes – photoelectric effect, Compton effect, and pair production. In energy analysis of γ-rays it is desirable to capture the total energy and to minimize the loss of energy by escape of the scattered γ-rays from Compton interaction.

This increases the number of events contributing to the photo peak which corresponds to the total γ-ray energy. Also, if lower energy γ-rays are present their photopeaks may be obscured by the Compton distribution from higher energy γ-rays. With anthracene crystals little resolution is seen in γ-spectra as the low atomic number of the absorber makes the principal interaction the Compton effect. However, in NaI(Tl), CsI(Tl), Si(Li), Ge(Li) and HPGe crystals the photoelectric effect is the more important. Increasing the size of the crystal increases the probability of photon capture and, therefore, the probability of capture of the scattered γ-ray in Compton events is increased. As a result, the increase in crystal size results in more capture of the total incident γ-ray energy which appears under the photopeaks.

For an ideal infinitely small detector a γ-spectrum from $^{137}$Cs would have the shape shown in Figure 8.19(a). For comparison theoretical γ-spectra for finite size and infinitely large detectors are shown in the same Figure. The counts located between the compton edge an photo peak for the medium size detector are due to multiple compton events. As can be seen detector size has a big influence of the Compton continuum and photo peak. A measured spectrum is shown in Figure 8.19(b). The energy of the compton edge, $E_{CE}$ (keV), caused by a γ-line of energy $E_\gamma$ (keV), is given by

$$E_{CE} = E_\gamma /[1 + 511/(2E_\gamma)] \tag{8.15}$$

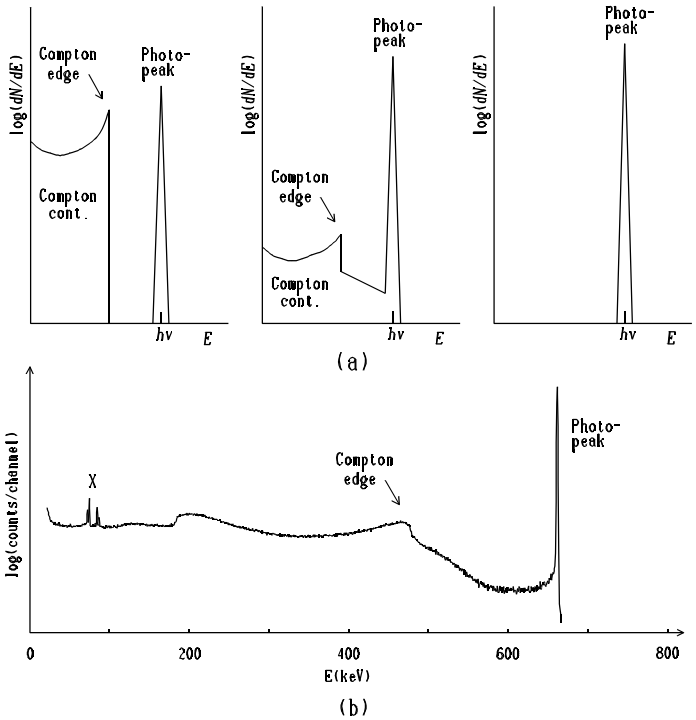


FIG. 8.19. (a) $^{137}$Cs γ-spectrum as calculated for "ideal" very small, medium and infinite size γ-detectors (b) the spectrum really recorded with a 22% HPGe detector.

where 511 is the energy in keV equivalent of one electron mass.

The broadening of the photo peak has many causes such as inhomogeneities in the crystals and variations in charge, or light, collection and noise in the preamplifier. However, for scintillation detectors the main cause is found in the PMT where nonuniformity in the photocathode, fluctuations in the high voltage imposed on each dynode, and statistical variations in the small number of photoelectrons formed at the photocathode are all contributing factors.

The resolution is the determining factor in the ability of the system to differentiate between photopeaks of γ-rays of similar energy. Other features of the spectrum in Figure 8.19(b) are the backscatter peak and the X-ray peaks. The broad backscatter peak, located between the X-rays and compton edge, arises by the absorption in the crystal of scattered photons resulting from γ-ray absorption via Compton interactions in the material surrounding the crystal. Obviously the magnitude of this peak is dependent on the distance of this material from the crystal and on the nature and amount of the material. The X-ray peaks (X in Figures 8.15 and 8.19(b)) are due to the absorption of the X-rays emitted in the electronic rearrangement following the nuclear disintegration, following internal conversion or after excitation of materials near the detector. Bursts of very low energy electrons are generated thermally in a semiconductor or emitted spontaneously from the photocathode in a PMT and are the cause of a noise peak at very low discriminator settings. This limits the photon energies that can be studied to a minimum of some thousand electron volts.

For γ-energies above 1.02 MeV, pair production in the detector followed by annihilation of the positron leads to the generation of pairs of 0.511 MeV photons. The probability increases rapidly with energy above 1.02 MeV. One or both of these photons may escape from the detector giving a deposited energy corresponding to the initial γ-energy less one or two times 0.511 MeV. Positrons are also generated outside the detector and their annihilation radiation reaches the detector. This gives rise to three smaller photo peaks called *escape peak*, *annihilation peak* and *double escape peak* at the corresponding energies, $E_\gamma - 0.511$ MeV, 0.511 MeV and $E_\gamma - 2 \times 0.511$ MeV, marked 1e, A and 2e respectively in Figure 8.15.

Coincident γ-rays emitted in rapid cascade during one decay may hit the detector at the same time and register as one event with the combined energy. This gives two effects, firstly the generation of a *sum peak* containing one count per coincidence and secondly corresponding loss of one count in each of the peaks corresponding to the coincident photons. Summing is strongly dependent on detector size and source to detector distance. Finally the coincidence may be purely random at high count rates, giving random summing between γ-rays of all occurring energies. In this case clear sum peaks will usually not be seen (except for sources having a few intense γ-lines), but the corresponding counts are still lost from respective photo peak.

The photo peaks from a well behaved detector are gaussians. Thus the FWHM value determines the peak shape. The energy scale is calibrated against standard isotopes and is normally almost linear. In most applications only the area below the photo peak but above the underlying continuum is used as a measure of activity. The total efficiency (based on photo peak area) varies usually with energy in the way illustrated by Figure 8.20.

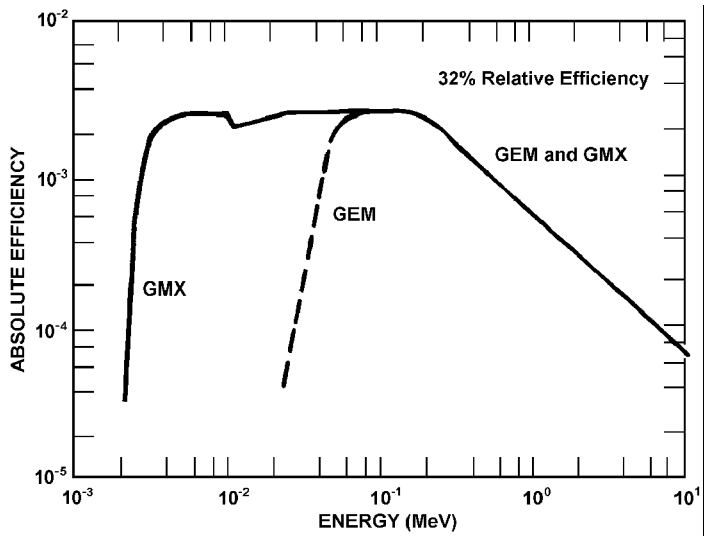


FIG. 8.20. Typical efficiency curves for HPGe detectors. GEM and GMX are detectors of n- and p-type with Be-window respectively. (Acc. to ORTEC.)

## 8.8. Special counting systems

For *low intensity measurements*, in which a level of radioactivity comparable to the normal background radiation is to be measured, special electronic circuits incorporating two detectors are used. The detectors are coupled so that a signal registers only when both detectors are activated at the same time (*coincidence circuit*) or, alternatively, when only one but not the other is activated at the same time (*anticoincidence circuit*). With such arrangements the normal β, γ background of a detector may be decreased by more than a factor of 100. In the most advanced coincidence techniques both detectors are energy sensitive as well, providing information on the type of radiation being measured. For example, β-γ coincidence measurements are used for absolute determination of radioactivity for samples in which β-decay is immediately followed by γ-emission.

Detectors which are *direction sensitive* have been developed primarily for use in medical diagnosis with radioactive isotopes. The simplest version involves a scintillation detector surrounded by a lead shield with a small hole (collimator) through which radiation reaches the detector. More complex systems with many detector/collimator pairs are in common use (γ-cameras); cf. §9.5. Scanning instruments (Fig. 9.13) have been developed which permit the measurement of radioactivity as a function of several coordinates as illustrated in Figure 9.14. Such instruments make it easy to detect the accumulation of a radioactive tracer in a particular organ of the body.

*Whole-body counters* were originally developed for investigation of poisoning by radioactive substances such as radium. They are now used diagnostically and consist of a large scintillation, or semiconductor, detector with the whole system, including the patient, placed in a heavily shielded room. The sensitivity is sufficient to measure natural radioactivity in the human body from such nuclides as $^{40}$K.

In nuclear installations like uranium mines, nuclear reactors, reprocessing plants, etc., it is necessary to continuously monitor gas and liquid effluents. Figure 8.21 shows an arrangement for monitoring of *radioactive aerosols* (e.g. Tc, Ru, actinides in air). Two detectors are used, so that some activity (e.g. mother or daughter activity) is allowed to decay between the two detectors. The delay time is adjusted by varying the length of the paper strip between the detector and the rate of movement of the paper strip. The detector may be energy sensitive or simple GM, proportional or scintillation devices. In monitoring of water the detectors (e.g. GM tubes) may dip into the streaming water, or the water may flow around the detector as in Figure 8.8(a).

*Radioactive gas flows* can be measured by using capillaries or packed columns of 2 – 20 ml volume containing scintillating material, either for monitoring purposes or, commonly, combined with a gas chromatograph for obtaining "radio-chromatograms" of $^{3}H$ or $^{14}C$ labeled organic substances. These detectors, which are commercially available, are viewed by PMTs connected to Personal-Computer (PC) based analysis and display systems.

*Radioactive liquid flows* can be monitored in several ways depending on the decay mode, energy and liquid film thickness. Liquid flow GM-counters (Fig. 8.8.a), or other types of flow cells combined with solid state detectors, are used at high β- and γ-energies. Glass scintillators embedded in tubings (alternatively tubings containing scintillators) are used for low-energy β-emitters (e.g. $^{3}H$, $^{14}C$, $^{35}S$). The flow cells have typically volumes from 0.01 to 5 ml. By using peak analysis (i.e. analyzing each scintillation intensity versus time, so-called "time-resolved technique") it is possible to measure α-emitters in high β-γ fluxes and even to obtain crude α-spectra, as well as to discriminate different β-emitters and to reduce background. A weakness of this technique is the memory effect in the detectors caused by radionuclide sorption. Therefore, the commercial systems have easily exchangeable flow cells. This demand is circumvented in the LISOL-system, in which the liquid flow is

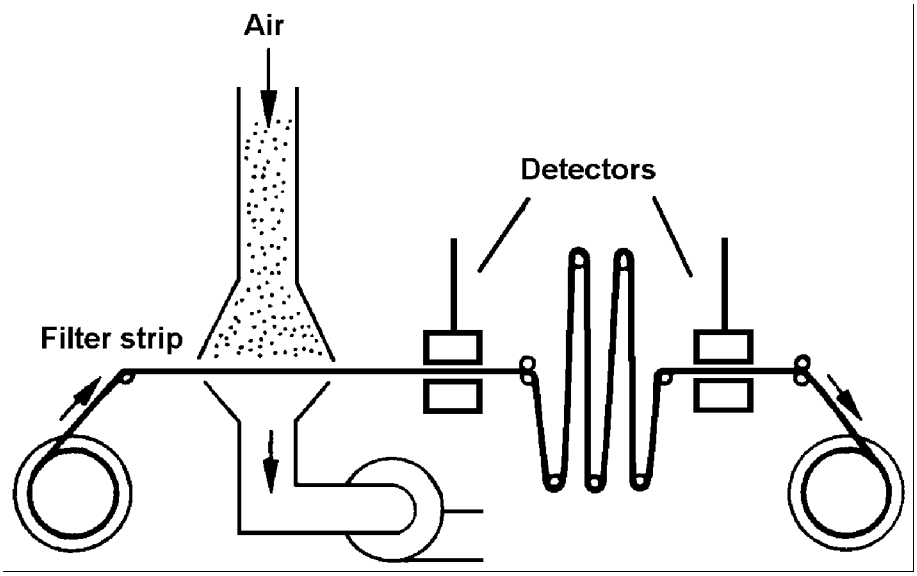


FIG. 8.21. Monitor for radioactive aerosols with prompt and delayed measurements. (From H. Kiefer and R. Maushardt.)

premixed with acid and scintillator solution before counting; the use of that system is described in §9.4.3.

## 8.9. Absolute disintegration rates

The determination of absolute disintegration rates is of great importance in all areas of nuclear chemistry, tracer work, age calculation, etc. Numerous methods have been employed, many using techniques described above, as track counting, liquid scintillation measurements, $4\pi$ proportional counters, etc. If the nuclei decay through $\beta$-$\gamma$ emission, the absolute rate may be obtained by two detectors placed close to each side of a thin sample, one detector $\beta$-sensitive and the other $\gamma$-sensitive.

When only a single detector in a conventional counting set-up is available (e.g. detector arrangement in Fig. 8.4), absolute counting rates can be obtained for unknown samples by comparison with known standards.

When standards are not available it is possible to obtain an approximate estimation of the absolute disintegration rate from a knowledge of the various factors that influence the counting efficiency. The detection efficiency $\psi$ is defined as a ratio between the count rate and the absolute disintegration rate (4.45). This detection efficiency, which was discussed briefly in §6.2, is the product of all the factors which influence the measured count rate and may be expressed as

$$\psi = \psi_{det}\psi_{res}\psi_{geom}\psi_{back}\psi_{self}\psi_{abs} \tag{8.16}$$

where $\psi_{det}$ = counting efficiency of detector,
$\psi_{res}$ = resolving time correction (see §8.3),
$\psi_{geom}$ = geometry factor (see §6.2),
$\psi_{back}$ = backscattering factor,
$\psi_{self}$ = self-absorption factor ($\psi_{sample} = \psi_{back}\psi_{self}$), and
$\psi_{abs}$ = absorption factor (see §6.2).

The efficiency of the detector is a measure of the number of counts registered compared to the number of particles that enter the sensitive volume of the detector. This efficiency is approximately 100% for $\alpha$- and high-energy $\beta$-particles in most detectors, but often substantially lower for $\gamma$-rays. Inasmuch as it is quite difficult to apply simple geometric considerations to the solid angle subtended by a detector for a source which is not concentrated at a point, usually the factors $\psi_{det}$ and $\psi_{geom}$ are determined experimentally by using a very thin standard source of approximately the same area as the unknown. The factor $\psi_{geom}$ can be calculated for circular samples and detector windows, see §6.2

It was noted in §6.4 that $\beta$-rays undergo large angle deflections. As a result, $\beta$-particles from the sample which may start in a direction away from detector can be deflected by several scattering events back into the detector. Such backscattering is dependent upon the atomic number of the material upon which the sample is supported (cf. Fig. 6.14). $\psi_{back}$ increases with backing material thickness up to a saturation thickness beyond which it is constant. Counting is usually done with either an essentially weightless backing ($\psi_{back} = 1$) or with a backing sufficiently thick as to have saturation. The saturation thickness

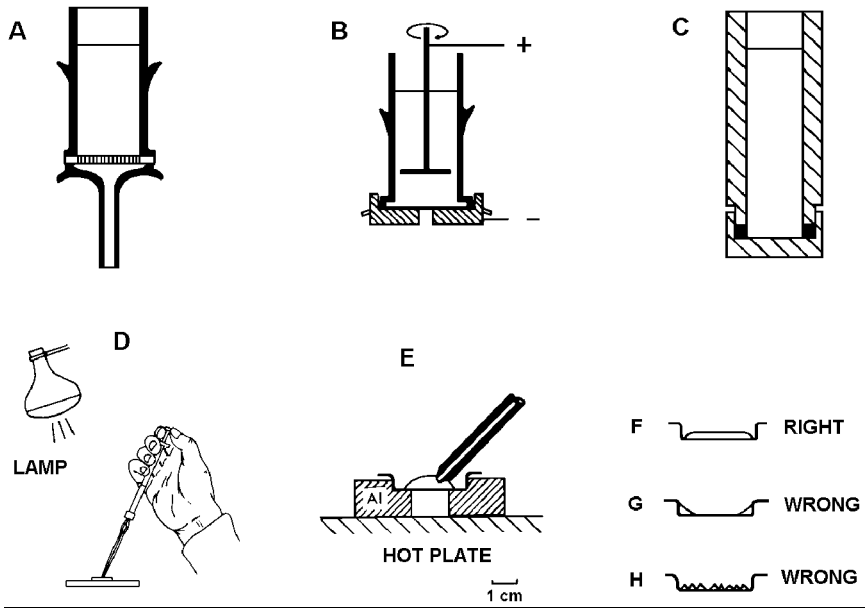


FIG. 8.22. The preparation of thin, uniform samples of known surface density. A, filtering arrangement; B, electrolytic plating system; C, centrifugation vessel; D–E, pipetting of a solution into an evaporation tray (glass, stainless steel, platinum), yielding a correct even deposit F or uneven samples G–H. The aluminum ring E should have a temperature only slightly exceeding the boiling point of the liquid.

corresponds to approximately 20% of the range of the β-particles in the backing material. Scattering can also occur from the walls of the sample holder, but this is usually less important than the backscattering from the sample backing material.

If the sample is thick, the count rate may be increased by internal backscattering, but the decrease of the count rate due to self-absorption within the sample is a greater factor. This sample self-absorption is inversely proportional to the β-ray energy and directly proportional to the thickness of the sample. For $^{32}P$ (1.72 MeV) sample thicknesses of 15 mg $cm^{-2}$ show little self-absorption, while for $^{14}C$ (0.15 MeV), the absorption for sample thicknesses as small as 1 mg $cm^{-2}$ is significant. The absorption factor can be determined by counting a series of samples of different thicknesses but with the same total disintegration rate, and then extrapolating that to zero sample weight.

The absorption factor $\psi_{abs}$ is related to the absorption of the particles after they leave the sample by any covering over the sample, by the air between the sample and the detector, by the absorption in the detector window, etc. Again, this factor is usually determined by experimental comparison with a sample of known absolute disintegration rate, a *standard*.

## 8.10. Sample preparation

From the discussion of the factors that enter into the counting efficiency it is obvious that the preparation of the counting sample must be done with care and must be reproducible if several samples are to be compared. Counting of α- and β-emitters *in solution* is best achieved by means of liquid scintillation counting. Because in this technique the emitters are included in the detection system itself the efficiency is very high and reproducible.

The advantage of using *solid samples* for counting is that the samples can be made very robust and small, allowing the use of either very simple counting systems (e.g. GM-counters), or the use of commercial very efficient high-capacity ( > 1000 samples/hour) automatic counting systems. Alpha-emitters can only be counted efficiently if the sample is very thin so that the self-absorbtion is eliminated. For α-spectrometry the surface density should be $< 0.1$ mg $cm^{-2}$. Preferably, α's should be counted by surface barrier detectors, windowless proportional counters or internal ion chambers. Counting of solid samples of β-emitters may or may not be a problem depending on the energy of the β-emission. Again, care must be taken with uniform thickness of sample, backscattering, etc. The use of energy sensitive detectors makes possible a reliable measurement of one particular radioactive nuclide in the presence of other radiation of secondary importance.

Solid samples can be prepared by a variety of techniques such as precipitation, evaporation, and electrolysis (Fig. 8.22). When the precipitation technique is used the radioactive material must always be precipitated for comparative counting with the same amount of carrier and all samples must have the same surface density. The precipitate is filtered on a filter plate or filter paper of known reproducible geometry A. If filtration is not feasible the precipitate may be centrifuged in special vials C, or the precipitate, after centrifugation and decanting, may be slurried with ether or alcohol, and the slurry transferred by pipette to a counting disc of fixed geometry; when the organic liquid evaporates, it hopefully leaves a uniform deposit of the precipitate slurry D, F. Problems are plentiful in obtaining a deposit of uniform thickness by evaporation of a solution. However, an arrangement such as that shown in Figure 8.22 E has been found to be suitable; slow and even evaporation of 0.1 – 1.0 ml samples result in an even deposit if the amount of solid material is small. More even deposits can be obtained by electro-deposition of samples from solution B. This method can be used also for nonaqueous solutions provided that the organic solvents contain traces of water and a potential of several hundred volts per centimeter is used. To speed-up sample preparation, different types of semi-automatic sample preparation systems are commercially available. They are particularly useful in bio-medical tracer research, where often large numbers of samples are produced.

## 8.11. Statistics of counting and associated error

Even if the experimental design and execution are perfect so that the determinant error is eliminated in experiments involving radioactivity there is always a random error due to the statistical nature of radioactive decay. Each radioactive atom has a certain probability of decay within any one time interval. Consequently, since this probability allows unlikely processes to occur occasionally and likely processes not to occur in any particular time interval, the number of decays may be more or less than the number in another similar

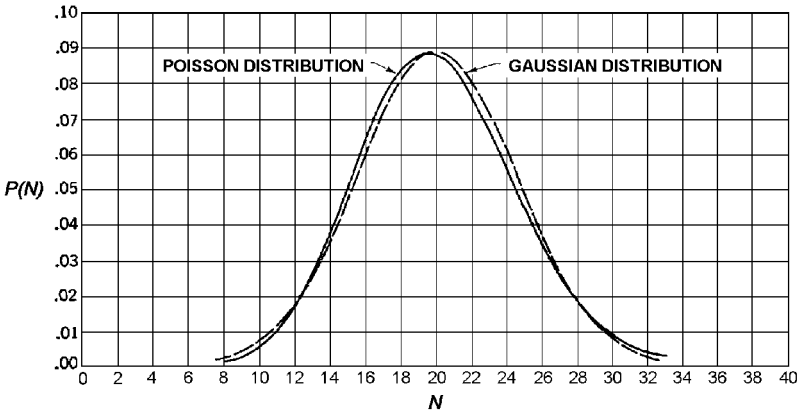


FIG. 8.23. Poisson (smooth) and Gaussian (dashed line) distributions for $\bar{N} = 20$.

interval for the same sample. It is necessary, when counting a sample, to be able to calculate the probability that the recorded count rate is within certain limits of the true (or average) count rate.

The binomial distribution law correctly expresses this probability, but it is common practice to use either the Poisson distribution or the normal Gaussian distribution functions since both approximate the first but are much simpler to use. If the average number of counts is high (above 100) the Gaussian function may be used with no appreciable error. The probability for observing a measured value of total count $N$ is

$$P(N) = (2\pi\bar{N})^{-\frac{1}{2}} e^{-\frac{1}{2}(\bar{N}-N)^2/\bar{N}} \tag{8.17}$$

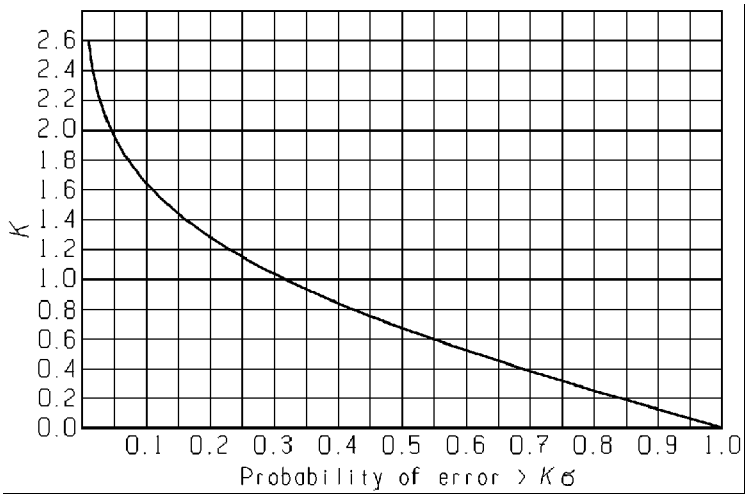


FIG. 8.24. The probability that an error will be greater than $K\sigma$ for different $K$-values.

The standard deviation σ is given in such cases by

$$\sigma = \sqrt{N} \tag{8.18}$$

In these equations $P(N)$ is the probability of the occurrence of the value $N$ while $\bar{N}$ is the arithmetic mean of all the measured values and $N$ is the measured value. Figure 8.23 shows the Poisson and Gaussian distributions for $\bar{N} = 20$ counts. The standard deviation ("statistical error"), according to the theory of errors, indicates a 68% probability that the measured value is within $\pm\sigma$ of the average "true" value $\bar{N}$. For 100 measured counts the value $100 \pm 10$ indicates that there is a 68% probability that the "true" value will be in the interval between 90 and 110 counts. If the error limit is listed as $2\sigma$ the probability that the "true" count will be between these limits is 95.5%; for $3\sigma$ it is 99.7%. Figure 8.24 shows the relationship between $K$, the number of standard deviations, and the probability that the true figure lies outside the limits expressed by $K$. For example, at $K = 1$ (i.e. the error is $\pm 1\sigma$) the figure indicates that the probability of the true" value being outside $N \pm \sigma$ is 0.32 (or 32%). This agrees with the observation that the probability is 68%, i.e. the "true" value is within the limits of $\pm 1\sigma$. Figure 8.24 can be used to establish a "rule of thumb" for rejection of unlikely data. If any measurement differs from the average value by more than five times the probable error it may be rejected as the probability is less than one in a thousand that this is a true random error. The probable error is the 50% probability which corresponds to $0.67\sigma$.

From the relationship of σ and $N$ it follows that the greater the number of collected counts the smaller the uncertainty. For high accuracy it is obviously necessary to obtain a large number of counts either by using samples of high radioactivity or by using long counting times.

In order to obtain the value of the radioactivity of the sample, corrections must be made for background activity. If our measurements give $N \pm \sigma$ counts for the sample and $N_0 \pm \sigma_0$ for the background count, the correct value becomes

$$N_{corr} = (N - N_0) \pm (\sigma^2 + \sigma_0^2)^{1/2} \tag{8.19}$$

If the sample was counted for a time $\Delta t$ and the background for a time $\Delta t_0$, the measured rate of radioactive decay is

$$R = N/\Delta t - N_0/\Delta t_0 \pm [(\sigma/\Delta t)^2 + (\sigma_0/\Delta t_0)^2]^{1/2} \tag{8.20}$$

It is extremely important in dealing with radioactivity to keep in mind at all times the statistical nature of the count rate. Every measured count has an uncertainty and the agreement between two counts can only be assessed in terms of the probability reflected in terms of σ.

The statistical nature of radioactive decay also leads to an uneven distribution of decays in time which is important when handling dead-time corrections and discussing required system time resolution. Let us first assume that a decay has occurred at time $t = 0$. What is then the differential probability that the next decay will take place within a short time interval, d$t$, after a time interval $t$ has passed? Two independent processes must then occur in series. No decay may take place within the time interval from 0 to $t$, probability $P(0)$,

followed by a decay within the time interval d$t$, probability $r$d$t$. The total probability is then given by the product of the individual probabilities of the two processes, i.e. if the combined probability is denoted $P(t)$d$t$ then

$$P(t)\mathrm{d}t = P(0) \times r\,\mathrm{d}t$$

By applying the Poisson distribution and noting that $r$ is equal to $\lambda N_0$ we obtain

$$P(t)\mathrm{d}t = \lambda N_0\, \mathrm{e}^{-\lambda N_o t}\,\mathrm{d}t = A_0\, \mathrm{e}^{-A_o t}\,\mathrm{d}t \tag{8.21}$$

In experimental work with radionuclides many other errors occur in addition to statistical error in the count rate. Such errors may originate in the weighing or volumetric measurements, pH determination, etc. Such errors must also be considered in presenting the final results. For such composite errors, the *law of error propagation* must be applied:

$$\sigma_F = [(\sigma_A\, \mathrm{d}F/\mathrm{d}A)^2 + (\sigma_B\, \mathrm{d}F/\mathrm{d}B)^2]^{½} \tag{8.22}$$

where $\sigma_F$ is the (one standard deviation) error in $F$, which is a function of the uncorrected variables $A$, $B$, …, with the standard errors $\sigma_A$, $\sigma_B$, etc. For the product $A.B$ and ratio $A/B$, one obtains

$$F = (A.B)\,(1 \pm s) \tag{8.23}$$

$$F = (A/B)\,(1 \pm s) \tag{8.24}$$

where

$$s = [(\sigma_A/\mathrm{A})^2 + (\sigma_B/\mathrm{B})^2]^{½} \tag{8.25}$$

For the function $A^x$ and log $A$ the following relations are valid

$$F = A^x \pm x.A^{x-1}\,\sigma_A \tag{8.26}$$

$$F = \log A \pm [\sigma_A/(2.303A)]^{½} \tag{8.27}$$

A useful technique for checking that the error in the measurements has a Gaussian distribution is the so-called "$\chi$-square" test. The quantity $\chi^2$ is calculated from

$$\chi^2 = \sum_{i=1}^{M} [(\bar{F} - F_i)^2]/[\bar{F}(k-1)] \tag{8.28}$$

where $M$ is the number of measurements (e.g. points on a curve) for which the function $F$ is (believed to be) valid. $\chi^2$ would have a value 0.5 – 1.0 when the Gaussian fit exceeds 50%. $k$ is the number of freedom, i.e. $M$ plus the number of independent variables. This relation is generally valid; for simple counting systems $F$ is replaced by $N$, the number of counts in a given time interval, and $k = M$.

## 8.12. Exercises

**8.1.** A detector has a 1 $cm^2$ efficient area perpendicular to a γ-particle flux produced by a source 7 m away. The sensitivity for the 0.73 MeV γ-radiation is 8.2%. (a) What must the source strength be for the detector to register 1000 cpm? (b) What fraction of the radiation is absorbed in the air space between source and detector?

**8.2.** A ~ 100 MeV fission fragment is stopped in a plastic plate with density ~ 1 and an average atomic spacing of 0.25 nm. Estimate (a) the range in the plate, and (b) the ionization density (ion pairs $\mu m^{-1}$). If the ionization along the track is spread out perpendicular from the track so that 1 in 10 atoms are ionized (c) what would be the diameter of the track? From the track dimensions (d) calculate the average energy deposition to each atom within the "cylinder", and, using the relation $E = 3\mathbf{k}T/2$, (e) estimate the average temperature within the track volume. In lack of basic data for the plastic material, use data for water.

**8.3.** Plutonium in an urine sample is soaked into a photographic emulsion so that the emulsion increases its volume by 20%. The 12 μm thick emulsion is dried to original thickness and then left in darkness for 24 h. After development, α-tracks are counted and an average of 2356 tracks $cm^{-2}$ found. If the plutonium consists of 67% $^{239}Pu$ and 33% $^{240}Pu$, what was the plutonium concentration in the urine?

**8.4.** A $^{244}Cm$ sample is measured in an ion chamber (Fig. 8.9). The voltage drop over a $3 \times 10^{13}$ Ω resistor is measured to be 0.47 V. What is the activity of the sample if all α's emitted in the chamber (2π geometry) are stopped in the gas?

**8.5.** In a proportional counter filled with methane of 1 atm the gas multiplication is $2 \times 10^4$. What is the maximum pulse size for a 5.4 MeV α, if the ion-pair formation energy is assumed to be 30 eV? The capacitance of the circuit is 100 pF.

**8.6.** In a GM counter, sample A gave 12630, B 15480, and A + B together 25147 cpm. (a) What is the resolving time of the counter? (b) With the same counter, the distribution of radioactive samarium between an organic phase and water was measured according to $D_m = R_{org}/R_{aq}$. The measured $R_{org}$ is 37160 cpm, and that of $R_{aq}$ is 2965. (b) What is the measured $D_m$? (c) Using corrections for resolving time, what is the true $D$-value?

**8.7.** Assume that $10^9$ alcohol molecules are dissociated per discharge in a GM tube of 100 $cm^3$ filled with 90% Ar and 10% ethyl alcohol vapor at a pressure of 100 mmHg (25°C). What is the lifetime of the tube in terms of total counts assuming this coincides with the dissociation of 95% of the alcohol molecules?

**8.8.** A 1 mm tick surface barrier detector of 10 mm diameter has a resistivity of 7000 Ω cm and a capacitance of 50 pF at 300 V reverse bias. Calculate the resolving time (time constant).

**8.9.** A plastic scintillation detector was to be calibrated for absolute measurements of β-radiation. For this purpose a $2.13 \times 10^{-5}$ M $^{204}TlCl_3$ solution was available with a specific activity of 13.93 $\mu Ci\ ml^{-1}$; $^{204}Tl$ emits β-particles with $E_{max}$ 0.77 MeV. Of this solution 0.1 ml is evaporated over an area of exactly 0.1 $cm^2$ on a platinum foil. The sample is counted in an evacuated vessel at a distance of 15.3 cm from the detector, which has a sensitive area of 1.72 $cm^2$. The detector registers 2052 cpm with a background of 6 cpm. What is (a) the surface weight of the sample, (b) the backscattering factor, and (c) the detector efficiency for the particular β's?

**8.10.** A sample counted for 15 min gave 9000 total counts. A 30 min background measurement registered 1200 counts. Calculate (a) the count rate or the sample alone, with its standard deviation, and (b) with its probable error.

**8.11.** A certain sample has a true average counting rate of 100 cpm. What is the probability that 80 counts would be obtained in a 1 min recording?

## 8.13. Literature

H. YAGODA, *Radioactive Measurements with Nuclear Emulsions*, Wiley, 1949.
G. B. COOK and J. F. DUNCAN, *Modern Radiochemical Practice*, Oxford University Press, 1952.
S. FLÜGGE and E. CREUTZ (Eds.), *Instrumentelle Hilfsmittel der Kernphysik II. Handbuch der Physik*, XLV, Springer-Verlag, 1958.
G. D. O'KELLEY, *Detection and Measurement of Nuclear Radiation*, NAS-NS 3105, Washington DC, 1962.
E. SCHRAM and R. LOMBAERT, *Organic Scintillation Detectors*, Elsevier, 1963.
W. H. BARKAS, *Nuclear Research Emulsions*, Academic Press, 1963.
W. J. PRICE, *Nuclear Radiation Detection*, McGraw-Hill, 1964.
P. C. STEVENSON, *Processing of Counting Data*, NAS-NS 3109, Washington DC, 1966.

W. B. MANN and S. B. GARFINKEL, *Radioactivity and its Measurement*, van Nostrand, 1966.
Nuclear spectroscopy instrumentation, *Nucl. Instr. Meth.* **43** (1966) 1.
G. BERTOLINI and A. COCHE (Eds.), *Semiconductor Detectors*, North-Holland, 1968.
R. J. BROUNS, *Absolute Measurement of Alpha Emissions and Spontaneous Fission*, NAS-NS 3112, Washington DC, 1968.
J. M. A. LENIHAN and S. J. THOMSON, *Advances in Activation Analysis*, Academic Press, 1969-.
K. BÄCHMANN, *Messung Radioaktiver Nuklide*, Verlag-Chemie GmbH , 1970.
C. E. CROUTHAMEL, F. ADAMS, and R. DAMS, *Applied Gamma Ray Spectrometry*, Pergamon Press, Oxford, 1970.
O. C. ALLKOFER, *Teilchen-Detectoren*, Thiemig, 1971.
P. QUITTNER, *Gamma Ray Spectroscopy*, Adam Hilger, London, 1972.
H. KIEFER and R. MAUSHART, *Radiation Protection Measurement*, Pergamon Press, Oxford, 1972.
R. A. FAIRES and B. H. PARKS, *Radioisotope Laboratory Techniques*, Butterworth, 1973.
J. A. COOPER, Comparison of particle and photon excited X-ray fluorescence applied to trace element measurements or environmental samples, *Nucl. Instr. Meth.* **106** (1973) 525.
J. KRUGERS, *Instrumentation in Applied Nuclear Chemistry*, Plenum Press, 1973.
*Users' Guide for Radioactivity Standards*, NAS-NS 3115, Washington DC, 1974.
D. L. HORROCKS, *Application of Liquid Scintillation Counting*, Academic Press, 1974.
P. J. OUSEPH, *Introduction to Nuclear Radiation Detection*, Plenum Press, 1975.
R. L. FLEISCHER, P. B. PRICE, and R. M. WALKER, *Nuclear Tracks in Solids*, University of California Press, 1975.
G. F. KNOLL, *Radiation Detection and Measurement*, 2nd Ed., John Wiley & Sons, 1989.
S. DEFILIPPIS, Activity analysis in liquid scintillation counting, *Radioactivity and Radiochemistry* **1**, 4 (1990) 22.